



Identification of novel 1,3-diaryl-1,2,4-triazole-capped histone deacetylase 6 inhibitors with potential anti-gastric cancer activity

Xin-Hui Zhang^{a,1}, Hui-Qin Kang^{a,1}, Yuan-Yuan Tao^a, Yi-Han Li^a, Jun-Ru Zhao^a,
Ya-Gao^{a,**}, Li-Ying Ma^{a,b,*}, Hong-Min Liu^{a,***}

^a Collaborative Innovation Center of New Drug Research and Safety Evaluation, Henan Province, Key Laboratory of Technology Drug Preparation (Zhengzhou University), Ministry of Education of China, Key Laboratory of Henan Province for Drug Quality and Evaluation, School of Pharmaceutical Sciences, Zhengzhou University, Zhengzhou, 450001, PR China

^b China Meheco Topfond Pharmaceutical Co., Ltd, Zhumadian, 463000, PR China

ARTICLE INFO

Article history:

Received 16 February 2021

Received in revised form

14 March 2021

Accepted 16 March 2021

Available online 31 March 2021

Keywords:

HDAC6

1,2,4-Triazole

Bioisostere

Gastric cancer

ABSTRACT

Histone deacetylase 6 (HDAC6) has emerged as a critical regulator of many cellular pathways in tumors due to its unique structure basis and abundant substrate types. Over the past few decades, the role played by HDAC6 inhibitors as anticancer agents has sparked great interest of biochemists worldwide. However, they were less reported for gastric cancer therapy. In this paper, with the help of bioisosteric replacement, in-house library screening, and lead optimization strategies, we designed, synthesized and verified a series of 1,3-diaryl-1,2,4-triazole-capped HDAC6 inhibitors with promising anti-gastric cancer activities. Amongst, compound **9r** displayed the best inhibitory activity towards HDAC6 ($IC_{50} = 30.6$ nM), with 128-fold selectivity over HDAC1. Further BLI and CETSA assay proved the high affinity of **9r** to HDAC6. In addition, **9r** could dose-dependently upregulate the levels of acetylated α -tubulin, without significant effect on acetylated histone H3 in MGC803 cells. Besides, **9r** exhibited potent antiproliferative effect on MGC803 cells, and promoted apoptosis and suppressed the metastasis without obvious toxicity, suggesting **9r** would serve as a potential lead compound for the development of novel therapeutic agents of gastric cancer.

© 2021 Elsevier Masson SAS. All rights reserved.

1. Introduction

Histone acetylation and deacetylation are widely occurring post-translational modification processes [1,2], which maintain the balance between nuclear and cytoplasmic protein acetylation levels, and are catalyzed by histone acetyltransferases (HATs) and histone deacetylases (HDACs), respectively [3] (Fig. 1A). To date, eighteen distinct HDACs have been identified in mammals. According to the sequence homology to yeast protein orthologs, they

are classified into four classes: class I (HDAC1, 2, 3, 8), class IIa (HDAC4, 5, 7, 9), class IIb (HDAC 6, 10), and class IV (sole HDAC11) are Zn^{2+} -dependent enzymes, whereas class III HDACs (sirtuins 1–7) are NAD^+ -dependent enzymes [4,5]. Noteworthy, the dysregulation of HDACs is closely related to the disruption of body homeostasis, leading to the development of human diseases, especially cancers [1]. HDAC inhibitors (HDACi) have been identified as effective anticancer agents by altering the acetylated status of various cellular proteins, increasing the expression levels of p21 and other genes, and inhibiting the proliferation of tumor cells via the induction of cellular differentiation or apoptosis [6]. Currently, four HDAC inhibitors, including vorinostat (SAHA), belinostat, panobinostat, and romidepsin, have been approved by FDA for the treatment of refractory or relapsed cutaneous and peripheral T cell lymphomas, or multiple myeloma [7], chidamide was another potent HDACi developed and approved in China for use in peripheral T cell lymphomas [8]. Moreover, they are all Zn^{2+} -dependent inhibitors, and their representative pharmacophores could be divided into three domains: Cap, Linker, and a zinc-binding group

* Corresponding author. Collaborative Innovation Center of New Drug Research and Safety Evaluation, Henan Province, Key Laboratory of Technology Drug Preparation (Zhengzhou University), Ministry of Education of China, Key Laboratory of Henan Province for Drug Quality and Evaluation, School of Pharmaceutical Sciences, Zhengzhou University, Zhengzhou, 450001, PR China.

** Corresponding author.

*** Corresponding author.

E-mail addresses: ya_gao@zzu.edu.cn (Ya-Gao), maliying@zzu.edu.cn (L.-Y. Ma), liuhm@zzu.edu.cn (H.-M. Liu).

¹ These senior authors contribute equally to this work.

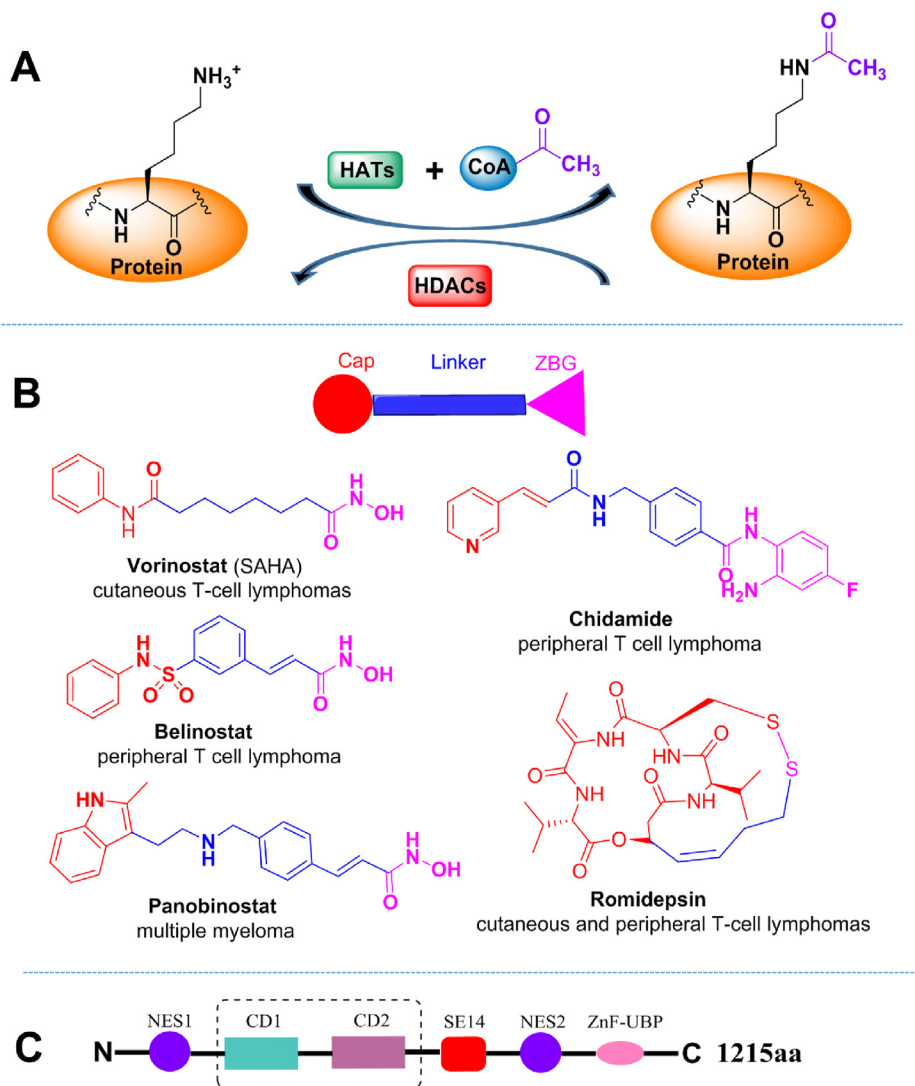


Fig. 1. (A) Acetylation and deacetylation, catalyzed by HATs and HDACs respectively, occur on specific lysine residues at histones *N*-terminal tails. (B) Current approved HDACis for cancer therapy in clinical, and their representative pharmacophore model: Cap, Linker and zinc-binding group (ZBG); (C) The architecture of HDAC6 functional domains. Reprinted with permission from *Journal of Medicinal Chemistry* [13], Copyright 2021, American Chemical Society.

(ZBG) (Fig. 1B). However, with the exception of romidepsin (selective HDAC1/2 inhibitor), the others are all lack of isoform selectivity, and have adverse side effects, such as fatigue, cardiotoxicity, thrombocytopenia, and bleeding in the gastrointestinal tract [9–11]. Therefore, interest is shifting towards the development of isoform-selective inhibitors [7,12,13].

HDAC6, the largest member of HDAC family, contains 1215 amino acid residues, two independent catalytic domains CD1 and CD2, which are located at the *N*-terminal and the central region, respectively [14,15] (Fig. 1C). In addition, the zinc-finger ubiquitin-binding domain (ZnF-UBP) at the C-terminal of HDAC6 mediates the interaction with the ubiquitin proteasome and aggresome pathway to clear misfolded proteins [16,17]. And, the nuclear export signaling (NES) part enables HDAC6 to translocate to the cytoplasm, and target non-histone substrates, such as α -tubulin [18,19], cortactin [20,21], heat shock protein (HSP90) [22,23] and peroxiredoxin [24]. Owing to its unique structure basis and abundant substrate types, HDAC6 plays a vital role in regulating cell proliferation, metastasis, invasion, and mitosis in the development of various tumors [15,25]. Over the past few decades, the role played by selective HDAC6 inhibitors as anticancer agents, either alone or

in combination with other approved drugs, has sparked great interest of biochemists worldwide [13,15]. However, for gastric cancer, which is a common malignancy as one of the leading causes of cancer-associated death in the world [26], even though the aberrant overexpression of HDAC6 is critical to the process of gastric carcinogenesis [27–29], there are fewer reports on HDAC6 inhibitors for the treatment of gastric cancer. Therefore, the development of HDAC6 inhibitors targeting gastric cancer appeared to be feasible and meaningful.

1,2,4-triazole, an integral pharmacophore of many clinically approved drugs, showed a broad range of biological functions, such as antibacterial, anxiolytic, antiparasitic, antitumor and antiviral activities [30–33]. Owing to its unique dipole properties and structural rigidity, 1,2,4-triazole exerts high affinity with the biological receptors via a variety of noncovalent interactions like π - π conjugation, hydrophobicity, electrostatic interactions, hydrogen bonding, and van der Waals force. In addition, 1,2,4-triazole nucleus is a recognized bioisostere of amides, esters, and carboxylic acids [33,34]. Intriguingly, the widely reported HDAC6 inhibitors, such as ricolinostat (ACY-1215), citarinosat (ACY-241), HPOB, HPB, and Nexturastat A, all share a common amide group in their scaffolds to

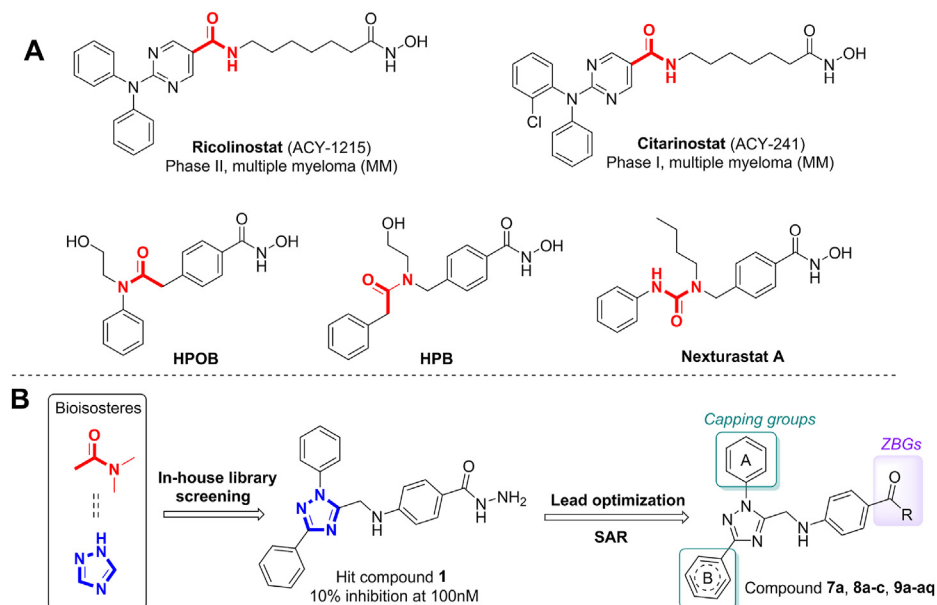


Fig. 2. (A) Representative selective HDAC6 inhibitors; (B) Lead optimization strategy based on the hit compound screened from our in-house library.

bridge the “Linker” and “Cap” portions (Fig. 2A). Thus, it appears that the active 1,2,4-triazole may be introduced into the backbones of these HDAC6 inhibitors to enhance their biological activities with the help of bioisosteric replacement strategy.

Fortunately, in our previous efforts, we have successfully developed series of 1,2,4-triazole derivatives as promising anti-cancer agents with impressive enzymatic activity and cytotoxicity [35–37], resulting in the building of an in-house library of compounds based on 1,2,4-triazoles, by which prompted us to search for new 1,2,4-triazole scaffolds as promising inhibitors for HDAC6. In this work, through an in-house library compounds screening, a hit compound **1** was picked out with potential inhibitory activity against HDAC6 (10% inhibition at 100 nM) (Fig. 2B). Further lead optimization strategy was adopted to design and synthesize a series of novel 1,3-diaryl-1,2,4-triazole derivatives based on compound **1**. Then, we performed detailed SAR studies, BLI and CETSA assay, as well as docking analysis to investigate the affinity of target compound with HDAC6. In addition, MTT method was used to test the antiproliferative effect of this class of HDAC6 inhibitors on gastric cancer cell line MGC803. Further mechanism studies confirmed the potential anti-gastric cancer activity of target compound.

2. Results and discussion

2.1. Chemistry

The general synthetic route of target 1,3-diaryl-1,2,4-triazole derivatives was shown in Scheme 1. Commercially available substituted phenylhydrazine **1a-p** were mixed with aromatic aldehyde **2a-ac** in ethanol water solution to obtain intermediate hydrazones **3a-aq** with more than 90% yield. Subsequently, in the presence of *tert*-butyl hydroperoxide (TBHP) and I_2 , **3a-aq** was involved in the ring-closure reaction with ethanolamine to get the 1,2,4-triazole scaffold **4a-aq** with 75%–85% yield. Then, compound **5a-aq** were produced by oxidizing **4a-aq** with Dess-Martin periodinane in a high yield (>95%). Next, with the help of Borch reductive amination, compound **5a-aq** were mixed with methyl 4-aminobenzoate in methanol, followed by adding catalytic amount

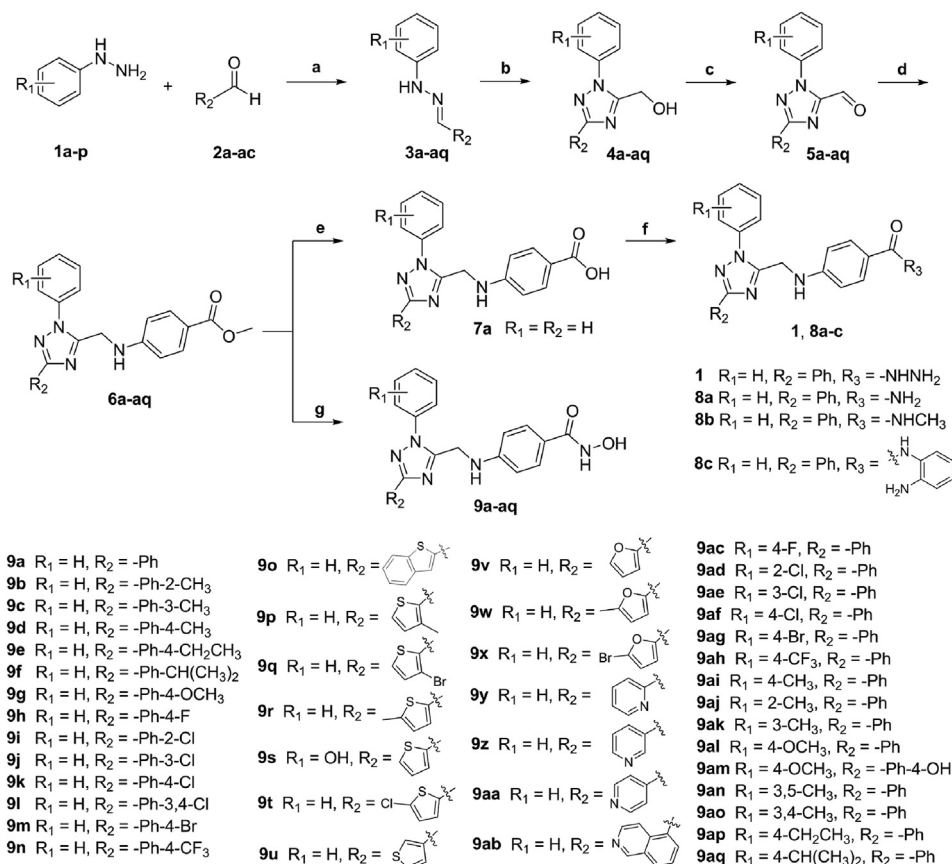
of acetic acid (AcOH) and sodium cyanoborohydride for a one-pot reaction to obtain compound **6a-aq** with the yield ranging from 65% to 75%. The intermediate ester **6a** were hydrolyzed under the action of sodium hydroxide to produce carboxylic acid product **7a** with high yield (95%), then condensed with the corresponding primary amine fragments to form the amide product **8a-c** and compound **1** in 60%–65% yield. In addition, target compound **9a-aq** could be obtained directly from **6a-aq** by hydrolysis of hydroxylamine with 75%–85% yield.

2.2. In vitro biological evaluations

2.2.1. Enzyme inhibition of target compounds towards HDAC6 and HDAC1

All the synthesized 1,3-diaryl-1,2,4-triazole derivatives were tested in vitro inhibitory activity towards HDAC6 and HDAC1. The pan-HDACi SAHA was selected as the control, and the preliminary evaluation showed the inhibition effect of compounds at a single concentration of 100 nM.

In our initial attempts, we have identified compound **1** as a hit compound from our in-house library screening, showing 10% inhibition towards HDAC6 at 100 nM. Meanwhile, we have reason to believe that the hydrazide moiety was responsible for the potential inhibitory efficacy of compound **1**, since the hydrazides have good zinc-binding ability and were widely used for the design of HDAC inhibitors [38,39]. Inspired by this progress, we firstly tried to optimize the “ZBG” portion of hit compound **1** by replacing with different ZBGs to explore the effect on efficacy. As shown in Table 1, when the hydrazide moiety was replaced with benzamide group, which was another potent ZBG present in the scaffold of HDACi chidamide [40], the inhibitory activity towards HDAC6 reduced moderately, while the potency against HDAC1 increased significantly (**8c** vs **1**). In addition, the replacements of carboxylic acid, amide, and *N*-methyl amide, all resulted in a dramatical loss of potency (**7a**, **8a**, **8b** vs **1**). Conversely, the hydroxamic acid moiety appeared to be a better alternative to enhance the activity, namely compound **9a**, showing more than 7-fold increase in the potency towards HDAC6, which might be attributed to the stronger zinc-binding ability of hydroxamic acid than hydrazide [41,42].



Scheme 1. Reagents and conditions: (a) AcOH, EtOH (20% wt), 80 °C; (b) ethanalamine, TBHP, I₂, MeCN, reflux; (c) Dess-Martin periodinane, DCM, 0 °C-rt; (d) AcOH, methyl 4-aminobenzoate, sodium cyanoborohydride, MeOH; (e) 1) sodium hydroxide, methanol, 70 °C; 2) formic acid, water. (f) 1) *tert*-Butyl carbazate, or *tert*-Butyl carbamate, or methylamine hydrochloride, or *N*-(*tert*-Butoxycarbonyl)-1,2-phenylenediamine, EDCl, HOBT, DCM, rt; 2) TFA, 1,4-dioxane; (g) 1) hydroxylamine (50% water), sodium hydroxide, DCM: MeOH = 1:2; 2) formic acid, water.

Table 1
Inhibitory effect of compounds **1**, **7a**, **8a-c**, **9a** against HDAC6 and HDAC1.

Compd.	R	HDAC6 inhibition ^a @ 100 nM (%)	HDAC1 inhibition ^a @ 100 nM (%)
1	-NHNH ₂	10.0	4.1
7a	-OH	-0.4	2.1
8a	-NH ₂	-4.4	-2.6
8b	-NHCH ₃	-3.6	-0.55
8c		5.0	32
9a	NHOH	72.6	19
SAHA	-	80.2	83.6

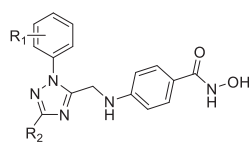
^a Data are represented as the mean of the inhibition rate.

Moreover, compared with SAHA, **9a** displayed higher selective inhibition for HDAC6 (72.6% for HDAC6, and 19% for HDAC1). In this view, compound **9a** was selected as the lead compound for further structural optimization. Likewise, the inhibition rates of derivatives

at a single concentration of 100 nM were summarized for primary SAR studies.

As shown in Table 2, we focused on optimizing compound **9a** by modifying its capping group composed of two aromatic regions

Table 2
Inhibitory effect of compounds **9a-aq** against HDAC6 and HDAC1.



Compd.	R ₁	R ₂	HDAC6 inhibition ^a @ 100 nM (%)	HDAC1 inhibition ^a @ 100 nM (%)
9a	H	Ph-	72.6	19.1
9b	H	2-CH ₃ -Ph-	53.2	16.5
9c	H	3-CH ₃ -Ph-	64.1	13.0
9d	H	4-CH ₃ -Ph-	62.2	20.3
9e	H	4-CH ₂ CH ₃ -Ph-	54.6	13.2
9f	H	4-CH(CH ₃) ₂ -Ph-	27.6	4.3
9g	H	4-OCH ₃ -Ph-	77.6	33.4
9h	H	4-F-Ph-	70.9	20.8
9i	H	2-Cl-Ph-	75.0	15.6
9j	H	3-Cl-Ph-	61.2	17.0
9k	H	4-Cl-Ph-	67.2	19.5
9l	H	3, 4-Cl-Ph-	34.5	7.6
9m	H	4-Br-Ph-	54.7	13.2
9n	H	4-CF ₃ -Ph-	41.6	4.9
9o	H		65.5	26.0
9p	H		72.1	26.3
9q	H		71.1	23.7
9r	H		79.7	30.1
9s	4-OH		79.6	38.4
9t	H		39.8	8.3
9u	H		53.4	15.2
9v	H		59.9	16.7
9w	H		60.7	22.3
9x	H		55.8	13.8
9y	H		58.6	16.0
9z	H		57.7	12.9
9aa	H		30.8	7.5
9 ab	H		40.2	11.2
9ac	4-F	Ph	67.6	16.3
9ad	2-Cl	Ph-	64.6	17.0
9ae	3-Cl	Ph-	62.3	14.7
9af	4-Cl	Ph-	55.4	18.0
9 ag	4-Br	Ph-	65.9	18.2
9ah	4-CF ₃	Ph-	38.9	12.8
9ai	4-CH ₃	Ph-	60.7	24.6

(continued on next page)

Table 2 (continued)

Compd.	R ₁	R ₂	HDAC6 inhibition ^a @ 100 nM (%)	HDAC1 inhibition ^a @ 100 nM (%)
9aj	2-CH ₃	Ph-	57.1	17.0
9ak	3-CH ₃	Ph-	66.0	18.4
9al	4-OCH ₃	Ph-	63.4	26.2
9am	4-OCH ₃	4-OH-Ph-	70.3	25.9
9an	3, 5-CH ₃	Ph-	49.8	12.4
9ao	3, 4-CH ₃	Ph-	53.0	11.0
9ap	4-CH ₂ CH ₃	Ph-	38.3	10.8
9aq	4-CH(CH ₃) ₂	Ph-	52.6	17.3
SAHA	—	—	80.2	83.6

^a Data are represented as the mean of the inhibition rate.

located in the N-1 and C-3 position of 1,2,4-triazole skeleton. To our delight, all the synthetic derivatives displayed better inhibition effect on HDAC6 than HDAC1, revealing the potential of this 1,3-diaryl-1,2,4-triazole-based chemical architecture for the design of selective HDAC6 inhibitors. In detailed, when the phenyl group at C-3 position was modified with different electron-donating groups, such as, methyl (**9d**), ethyl (**9e**), and isopropyl (**9f**), the activity showed a downward trend as the steric volume of the alkyl substituents increased (down from 62.2% to 27.6%). While, the modification of methoxyl led to a modest increase in activity (**9g**, up to 77.6% at 100 nM). Likewise, the activity of compound **9h**, **9m**, **9k**, and **9n** which were substituted by increasing bulky electron-withdrawing groups F, Cl, Br, and CF₃, respectively, showed a reduced trend (down from 70.9% to 41.6%). Meanwhile, it was also observed that double substitutions on the phenyl was unfavorable for the efficacy (**9l** < **9i**, **9j**, **9k**). In addition, we did observe that the changes of modification sites on phenyl group have less effect on activity, irrespective of the types of substituents (**9b** vs **9c** vs **9d**; **9i** vs **9j** vs **9k**). These results indicated the modification of the C-3 phenyl showed much preference to the steric hindrance of substituents, which might be explained by the reason that inhibitors bearing properly sized capping groups could comfortably occupy the surface groove of HDAC6 catalytic pocket well, without a steric clash with the residues [43].

With this in mind, several aromatic heterocycle groups, including benzothienyl, thienyl, furyl, pyridyl, and quinazoliny, were introduced to further explore the potential effect of modifications at C-3 position of 1,2,4-triazole. As shown in Table 2, the potency of these heterocyclic substituents differed substantially. In particular, thienyl appeared to be more favorable for the activity, and most compounds exerted more than 71% inhibition rate at 100 nM towards HDAC6. Amongst, compounds **9r** (79.7%) and **9s** (79.6%) bearing 5-methylthiophene-2-yl and thiophen-2-yl substituents, respectively, exhibited superior inhibition effect close to that of SAHA (80.2% for HDAC6). However, furyl substituent did not give too much breakthrough in activity (**9v-x** < 60%). In addition, the compounds displayed diminished activity after pyridyl modifications, including pyridin-2-yl (**9y**, 58.6%), pyridin-3-yl (**9z**, 57.7%), and pyridin-4-yl (**9aa**, 30.8%), which might be due to the lower hydrophobicity of pyridyl than phenyl [43]. Besides, the activity of compound **9ab** (40.2%) bearing quinazoliny also attenuate remarkably.

To expand the structural optimization, we further investigated the modifications of the phenyl located in N-1 position of 1,2,4-triazole. Unfortunately, these compounds (**9ac-aq**) all displayed lower activity than lead compound **9a**. Noteworthy, compared with electron-withdrawing groups, N-1 phenyl appeared to be more sensitive to the electron-donating substituents. For instance, compound **9ac-ag** containing F, Cl, and Br modifications showed little difference in activity. By contrast, the activity of compounds bearing methyl, ethyl, and isopropyl substituents presented a reduced trend (**9ai** > **9ap** > **9aq**), which was similar to

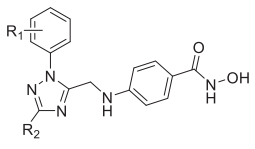
above-mentioned C-3 phenyl modification. Likewise, double substitutions on the phenyl proved to be adverse for the activity (**9ai-ak** > **9an** and **9ao**). In addition, the modifications of N-1 phenyl showed little preference to the substituent sites (**9ad** vs **9ae**, **9af**; **9ai** vs **9aj**, **9ak**). Ultimately, the inhibitory effect of compound **9a-aq** against HDAC6 at 100 nM concentration were ranked from highest to lowest (Fig. S1 in Supporting Information). And, compounds with >60.0% inhibition against HDAC6 were selected for further evaluation of their half-maximal inhibitory concentration (IC₅₀) values towards HDAC6 and HDAC1, respectively, as well as the selectivity index. The results were summarized in Table 3.

Consistent with above SAR studies, all chosen compounds showed potent inhibitory activity towards HDAC6 with IC₅₀ values at low sub-micromole levels, and almost always better selectivity indexes than SAHA (2.7-fold). Amongst, the lead compound **9a** displayed potent inhibitory activity against HDAC6 (IC₅₀ = 111.7 nM), showing more than 22-fold selectivity over HDAC1. In addition, it was worth nothing that modifications at C-3 phenyl of 1,2,4-triazole did not bring much improvement in activity (**9h**, IC₅₀ = 114.5 nM; **9j**, IC₅₀ = 114.6 nM). In contrast, they may cause diminished efficacy (**9a** vs **9c**, **9d**, **9g**, **9i**, **9k**). In addition, N-1 phenyl modification appeared to be more detrimental for the activity, resulting in weak IC₅₀ values for most compounds (**9ac-ae**, **9ag**, **9ai**, **9ak**), and poor selectivity (Index < 10-fold). Nevertheless, we did observe that thienyl modifications of C-3 position could significantly enhance the activity. In particular, compounds **9p** (IC₅₀ = 30.68 nM) and **9r** (IC₅₀ = 30.6 nM) exhibited more than 3-fold increase in activity than **9a**, and excellent selectivity for HDAC6 over HDAC1 (Selectivity index > 100). Notably, in comparison to the control Tubastatin A, which is a famous selective HDAC6 inhibitor [44], compound **9r** not only exerted more potent inhibitory activity against HDAC6, but also higher selectivity (index = 128.8). Above all, the SAR studies on the whole target derivatives could be summarized in Fig. 3.

2.2.2. The selected HDAC6 inhibitors inhibit the proliferation of MGC803 cells

As mentioned above, HDAC6 played an important role in the process of gastric carcinogenesis [27–29], and the inhibition of HDAC6 may trigger cell apoptosis, inhibit motility ability, and induce senescence and mitotic catastrophe in gastric cancer cells [45,46]. Herein, we attempted to verify the anti-gastric cancer activities of these HDAC6 inhibitors by choosing gastric cancer cell line MGC803 as a mode with MTT method. The results of Table 4 showed most of them could significantly inhibit the proliferation of MGC803 cells with IC₅₀ values ranging from 5.76 to 17.70 μM. Particularly, compound **9r** with the best potency and selectivity towards HDAC6 exhibited impressive antiproliferative activity against MGC803 cells with IC₅₀ value of 8.45 ± 0.93 μM, which was somewhat comparable with SAHA (IC₅₀ = 8.67 ± 0.93 μM). Likewise, compound **9p** also displayed similar inhibition effect. However, we did observe that compounds **9j**, **9k**, and **9q** had lower

Table 3
Inhibitory profile of selected target compounds against HDAC6 and HDAC1 (IC₅₀, nM).



Compd.	R ₁	R ₂	IC ₅₀ ^a (nM)		Selectivity index HDAC1/6
			HDAC6	HDAC1	
9a	H	Ph-	111.7	2488	22.3
9c	H	3-CH ₃ -Ph-	280.5	5522	19.7
9d	H	4-CH ₃ -Ph-	223.6	3099	13.9
9g	H	4-OCH ₃ -Ph-	163.2	2860	17.5
9h	H	4-F-Ph-	114.5	3400	29.7
9i	H	2-Cl-Ph-	184.6	3831	20.8
9j	H	3-Cl-Ph-	114.6	1873	16.3
9k	H	4-Cl-Ph-	180.7	2424	13.4
9o	H		323.6	1457	4.5
9p	H		30.68	3200	104.3
9q	H		54.94	2084	37.9
9r	H		30.6	3941	128.8
9s	4-OH		33.53	1502	44.8
9ac	4-F	Ph-	273.6	1818	6.6
9ad	2-Cl	Ph-	668.9	3118	4.7
9ae	3-Cl	Ph-	678.3	4396	6.5
9 ag	4-Br	Ph-	1729	3199	1.9
9ai	4-CH ₃	Ph-	309.7	1717	5.5
9ak	3-CH ₃	Ph-	388.2	3850	9.9
9 al	4-OCH ₃	Ph-	126.9	882.8	7.0
9am	4-OCH ₃	4-OH-Ph-	102.4	4303	42.0
SAHA	—	—	59.3	162.7	2.7
Tubastatin A	—	—	64.04	7048	110.1

^a IC₅₀ values for enzymatic inhibition of HDAC enzyme.

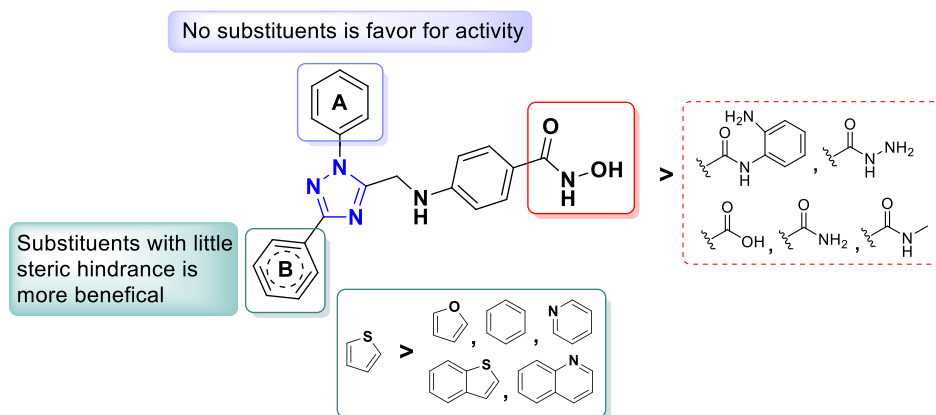


Fig. 3. The summary of SAR studies on the target compounds.

HDAC6 potency and selectivity than **9r**, while much better cytotoxicity. In contrast, compound **9d**, **9g** did not show obvious inhibition effect on the proliferation of MGC803 cells. On the other hand, compound **9o**, **9ac-ae**, **9 ag**, **9ai**, **9ak**, and **9 al**, bearing weak

selectivity indexes that were similar to SAHA lower than 10-fold, displayed moderate antiproliferative activity against MGC803 cells with IC₅₀ values ranging from 6.11 to 13.73 μM. These results suggested the dual inhibition of HDAC1/6 would lead to somewhat

Table 4
In vitro antiproliferation assay against MGC803 cells.

Compd.	IC ₅₀ ^a (μM)		
	MGC803	MGC803	
9a	17.70 ± 1.24	9r	8.45 ± 0.93
9c	8.71 ± 0.25	9s	>20
9d	>20	9ac	10.53 ± 1.48
9g	>20	9ad	9.63 ± 0.97
9h	8.96 ± 0.96	9ae	13.73 ± 1.36
9i	>20	9ag	9.30 ± 1.87
9j	5.76 ± 0.76	9ai	12.29 ± 0.51
9k	5.97 ± 0.38	9ak	13.21 ± 2.94
9o	6.11 ± 0.69	9al	7.05 ± 0.44
9p	8.89 ± 0.95	9am	>20
9q	6.32 ± 0.81	SAHA	8.67 ± 0.93

^a IC₅₀ values for proliferation inhibition of MGC803. Data are presented as the means ± SDs. All experiments were carried out at least three independent times.

better cytotoxicity towards MGC803 cells compared with selectively inhibiting HDAC6 alone, which might be attributed to the fact that HDAC1 also played an important role in the process of gastric cancer [47–49]. Given its superior HDAC6 potency and moderate antiproliferative activity against MGC803 cells, compound **9r** was selected to further explore its binding affinity with HDAC6 and in-depth anti-gastric cancer mechanism.

2.2.3. In vitro HDAC isoform selectivity assay for compound **9r**

To further explore the HDAC isoform selective profiles of compound **9r**, we additionally evaluated its inhibitory activity against HDAC2, HDAC3 and HDAC8. As shown in Table 5, compound **9r** displayed similar inhibition effect on these three isoforms, with IC₅₀ values of 224, 235 and 349 nM, respectively, which were all weaker than the inhibitory activity towards HDAC6. Meanwhile, in comparison to SAHA, **9r** showed better selective inhibition effect on HDAC6. These results suggested compound **9r** showed high HDAC6 selectivity over other isoforms, especially HDAC1 (Selectivity index > 128-fold).

2.2.4. Specific binding of compound **9r** to HDAC6 in vitro

Through the application of BLI, which is a new technology to explore the interaction between biological macromolecules with small molecules, it was fully proved that compound **9r** and human recombinant HDAC6 protein had strong binding affinity in vitro. The equilibrium dissociation constant (K_d) of **9r** to HDAC6 is 7.1 ± 0.9 nM (Fig. 4A and B). Additionally, cell thermal migration assay (CETSA) is a method based on the biophysical principle of ligand induced thermal stability of target protein to detect the binding ability of compounds to target protein in cells at the cellular level. As shown in Fig. 4C and D, compound **9r** increased the thermal stability of HDAC6 protein in MGC803 cells, and increased its tolerance temperature from 44 °C upper than 54 °C. These data indicated that **9r** could penetrate the cell membrane into the MGC803 cells, bind with HDAC6 protein, confirming the targeting of HDAC6. In order to discuss the inhibitory effect of **9r** on HDAC6 in more depth, we observed the changes of HDAC6 substrates by Western blot to prove the affinity of **9r** to HDAC6. The result is

Table 5
In vitro HDAC isoform selective profiles of compound **9r**.

Compd.	IC ₅₀ ^a (nM)					Selectivity index			
	HDAC1	HDAC2	HDAC3	HDAC6	HDAC8	HDAC1/6	HDAC2/6	HDAC3/6	HDAC8/6
9r	3941	224	235	30.6	349	128.8	7.3	7.7	11.4
SAHA	162.7	27	41	59.3	645	2.7	0.45	0.69	10.8

^a IC₅₀ values for enzymatic inhibition of HDAC enzyme.

shown in Fig. 4E and F, compound **9r** significantly leads to the accumulation of acetylated α-tubulin (Ac-α-tubulin) in a dose dependent manner without significantly increasing acetylation of histone H3, a major substrate of class I HDACs in MGC803 cells. Thus, our results indicated that **9r** is a selective HDAC6 inhibitor that selectively inactivates HDAC6 in human gastric cancer cells.

2.2.5. Molecular docking study

To get a better understanding of the behavior of the compound **9r** showing impressive affinity and selectivity to HDAC6, we performed molecular docking study to explore the binding models of **9r** within zebrafish HDAC6 CD2 (PDB code 5EF7, 1.9 Å) by using Molecular Operating Environment (MOE) software. As shown, compound **9r** fitted well into the hydrophobic pocket and exhibited a unique monodentate hydroxamate-Zn²⁺ coordination geometry related to phenylhydroxamate HDAC6 inhibitors (Fig. 5A and B) [50,51]. The hydroxamate N–O[−] group of **9r** coordinated with Zn²⁺ directly (Zn²⁺ ... O distance, 1.57 Å), along with the synergistic Zn²⁺ coordinations of D612, H614, and D705 residues in the bottom of HDAC6 catalytic channel. While the C=O group formed a hydrogen bond with Zn²⁺-bound water molecule with O...H separation of 2.06 Å. In addition, the phenyl-based linker of **9r** nestled in the hydrophobic tunnel, and was sandwiched between F583 and F643, engaging in a π-π stacking interaction. Notably, the NH group formed a moderate hydrogen bonding interaction with S531 residue (2.42 Å), which was confirmed to be a unique “gatekeeper” residue located at the mouth of HDAC6 CD2 active site conferring HDAC6 affinity and selectivity, that can be used to design specific HDAC6 inhibitors targeting this residue that is absent in other isozymes (Fig. 5A and B) [50]. Besides, it was not observed significant intermolecular interactions between the “Y”-shaped 1,2,4-triazole-based capping group of **9r** and the surface of HDAC6 catalytic pocket, except for the phenyl group was oriented toward the L1 loop pocket delineated by residues H463, P464, F583, and L712 (Fig. 5C), which might be explained by the fact that enzyme-inhibitors association appeared to be driven primarily by steric complementarity between the capping groups and the three-dimensional contours of the loop pockets in the active site of HDAC6 [51].

2.2.6. Compound **9r** induces apoptosis of MGC803 cells

In order to further explore the inhibitory activity of compound **9r** on MGC803 cell growth, we first detected the effect of **9r** on cell apoptosis by flow cytometry, and treated MGC803 cells with 0, 4 and 8 μM of **9r**, respectively. Flow cytometry analysis showed that **9r** induced early and late apoptosis of MGC803 cells by 2.93% and 54.41% respectively, while the apoptosis rate of MGC803 cells with DMSO was only 2.83% (Fig. 6A), indicating **9r** could enhance the apoptosis rate of MGC803 cells in a dose-dependent manner. Besides, Western blot showed that with the concentration of **9r** increasing, the anti-apoptosis protein Bcl-2 was down-regulated, and caspase-9, PARP showed a significant elevation in a dose-dependent manner (Fig. 6B and C). These findings suggested compound **9r** induced MGC803 cell apoptosis potentially via mitochondria-mediated pathways.

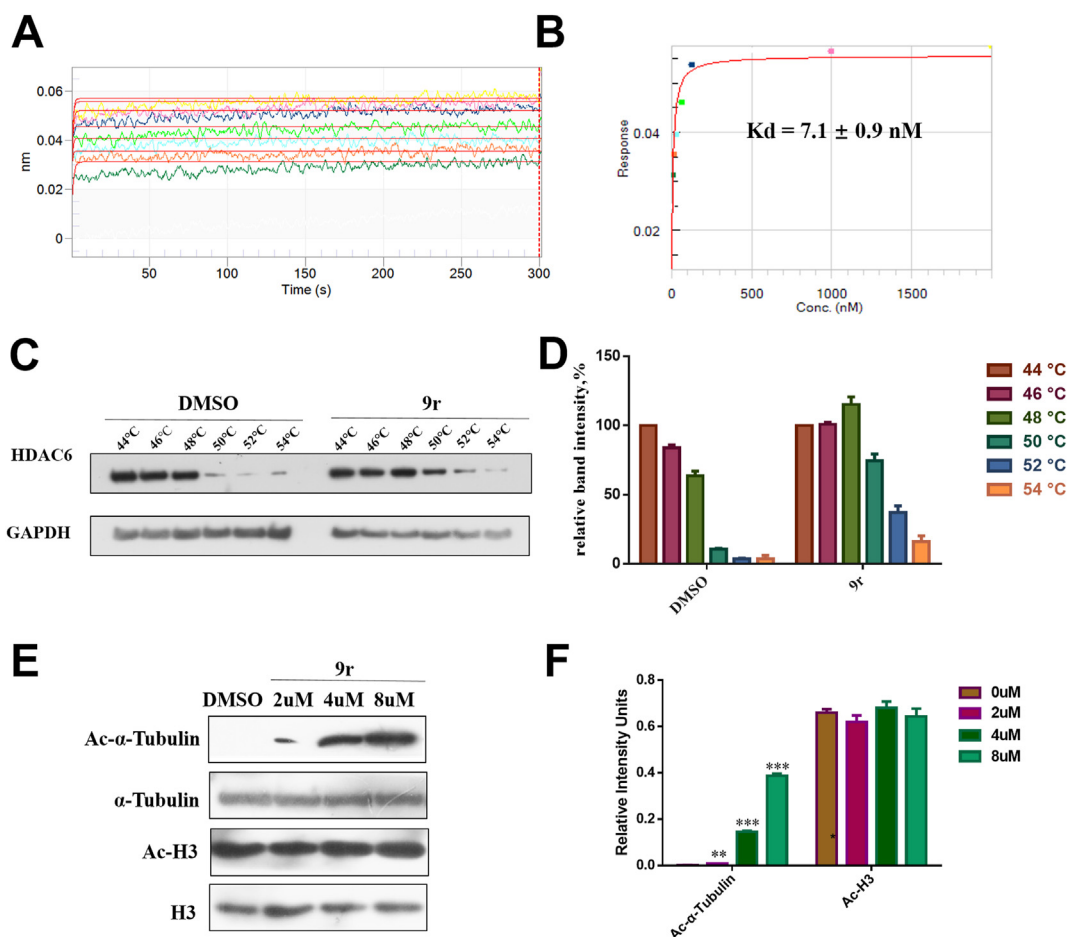


Fig. 4. The specific binding of compound **9r** to HDAC6 in vitro. (A, B) Measurement of affinity between **9r** with HDAC6 was carried out by BLI. The dissociation constant K_d values were automatically calculated by using Pall-ForteBio. (C, D) CETSA confirmed the binding capacity of **9r** with HDAC6 at cellular level. It is predictable that the specific binding of compound **9r** with HDAC6 protein in MGC803 cells. (E, F) The levels of the acetylation of α -tubulin and histone H3 after treated with **9r** in MGC803 cells at different concentrations were analyzed by Western blot. Data was shown as mean \pm SD from three independent experiments.

2.2.7. Compound **9r** inhibits cell proliferation and invasion

EdU staining showed that compound **9r** could significantly inhibit the proliferation of MGC803 cells (Fig. 7A and B). Additionally, transwell assay showed that compared with the DMSO, the treatment of **9r** significantly decreased the invasion rate of MGC803 cells in a dose-dependent manner (Fig. 7C and D).

2.2.8. Safety evaluation of compound **9r** by acute toxicity assay

In order to evaluate the safety of compound **9r**, acute toxicity assay was carried out. Mice were given 2 g/kg by gavage at one time and fed and observed normally for 14 days. During this period, not only did the mice in the **9r** treatment group survive, but they also maintained their weight without any obvious behavioral abnormalities (Fig. 8A). Additionally, the staining of normal tissues of mice in each group also showed no damage to normal tissues (Fig. 8B). Based on these experimental results, compound **9r** has no toxic effect on tissues at 2 g/kg in vivo, which fully proves the accuracy of a series of anti-tumor activity evaluation and the safety of the experimental dose.

3. Conclusions

Above all, with the help of bioisosteric replacement, in-house library screening, and lead optimization strategies, we have

designed, synthesized and verified a series of phenylhydroxamate HDAC6 inhibitors bearing 1,3-diaryl-1,2,4-triazole-derived capping groups. SAR studies showed the embellishment of two aromatic rings at N-1 and C-3 position of 1,2,4-triazole backbone was key for HDAC6 potency. Amongst, compound **9r** bearing a methyl-substituted thienyl at C-3 site displayed the best inhibitory activity towards HDAC6 ($IC_{50} = 30.6$ nM), with 128-fold selectivity over HDAC1. Docking studies disclosed the behavior of **9r** showing impressive affinity to HDAC6, that was also proved by BLI and CETSA assay. In addition, **9r** could dose-dependently upregulate the levels of acetylated α -tubulin, without significant effect on acetylated histone H3 in MGC803 cells. Cellular assay displayed **9r** exhibited potent antiproliferative effect on gastric cancer cell line MGC803. And in-depth investigation demonstrated it was involved in inhibiting MGC-803 cells proliferation, inducing mitochondria-related apoptosis and suppressing the metastasis ability of MGC803 cells. What need to be emphasized is that **9r** did not show any obvious toxicity in acute toxicity test, predicting a favorable treatment window of **9r**. Taken together, our studies provided a series of novel HDAC6 inhibitors, especially **9r**, with high selectivity towards HDAC6 over HDAC1, showed promising anti-gastric cancer activity, and warranted further exploration as a potential lead compound for the development of novel therapeutic agents of gastric cancer.

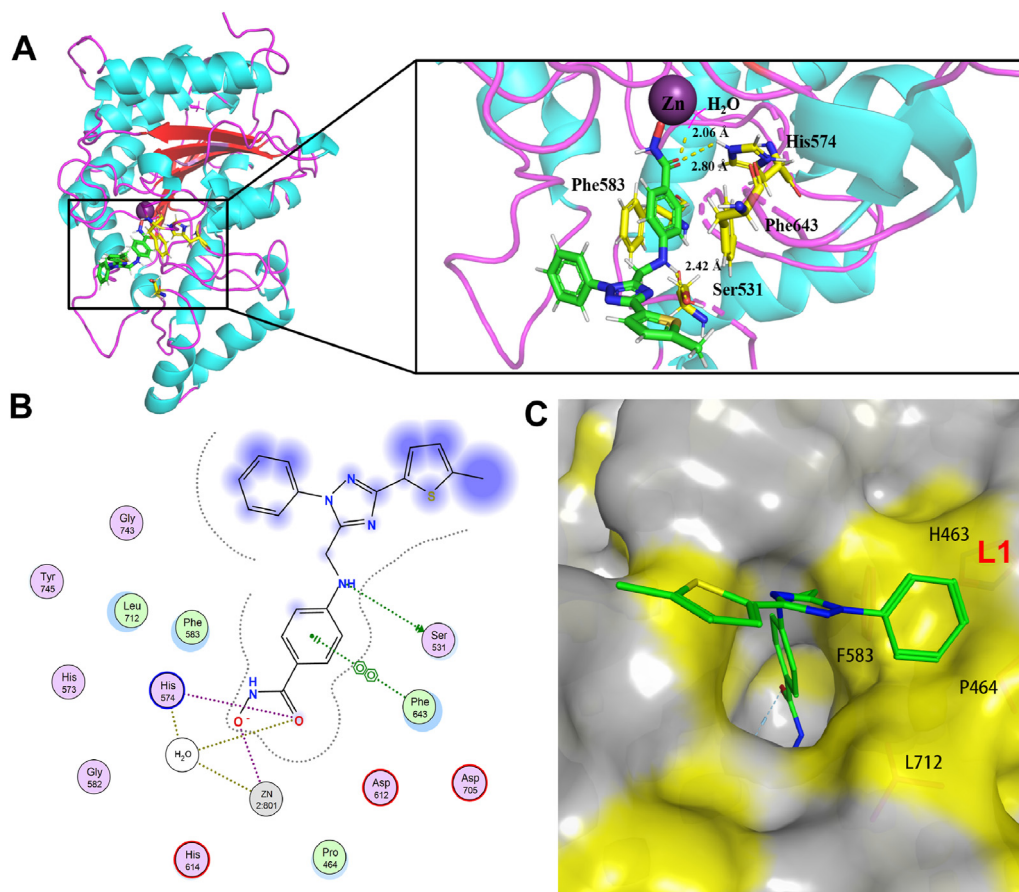


Fig. 5. (A) Predicted binding mode of **9r** docked into the active pocket of zebrafish HDAC6 CD2 (PDB code 5EF7, 1.9 Å); (B) Two-dimensional binding view of **9r** in HDAC6 CD2 active site; (C) The 1,2,4-triazole-based capping group of **9r** is oriented toward the L1 loop pocket delineated by residues of H463, P464, F583, and L712 (right part, colored yellow).

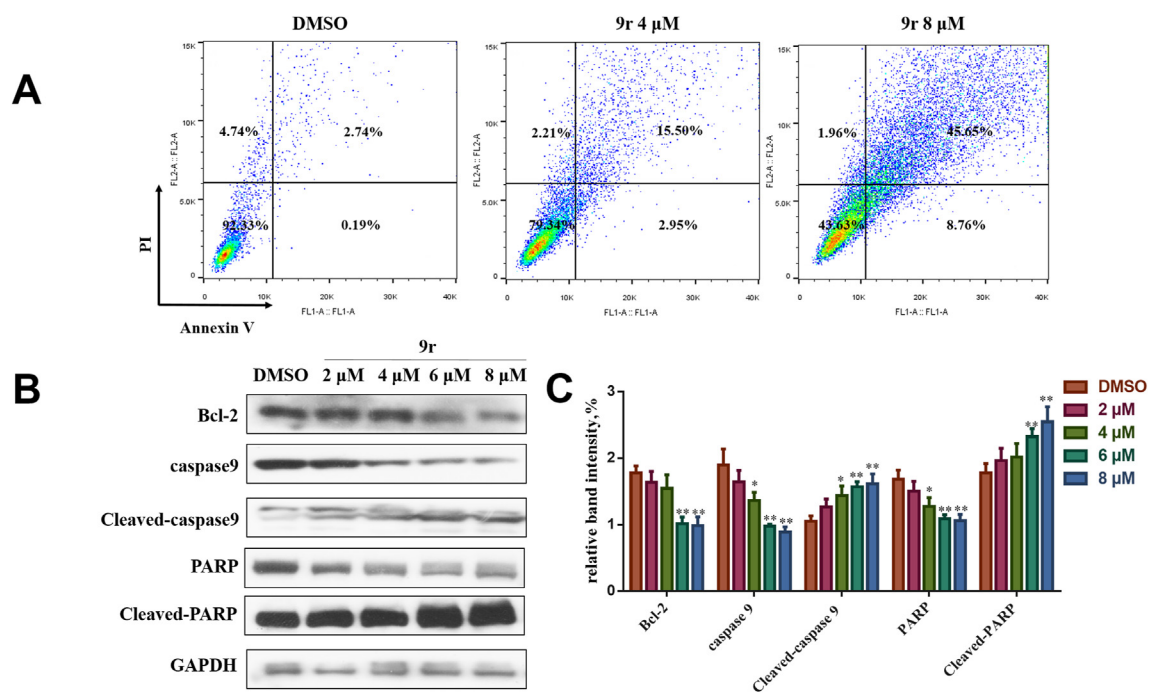


Fig. 6. Compound **9r** induced apoptosis in MGC803 cells. (A) MGC803 cells were treated with 0, 4 or 8 μM of **9r** and then processed for FACS by using Annexin V/PI staining. (B, C) The expression level of Bcl-2, caspase 9, PARP in mitochondria-related apoptosis pathway in MGC803 treated by compound **9r** or DMSO was analyzed and GAPDH was used as control. Data was shown as mean ± SD from three independent experiments. *p < 0.05, **p < 0.01 compared with the control.

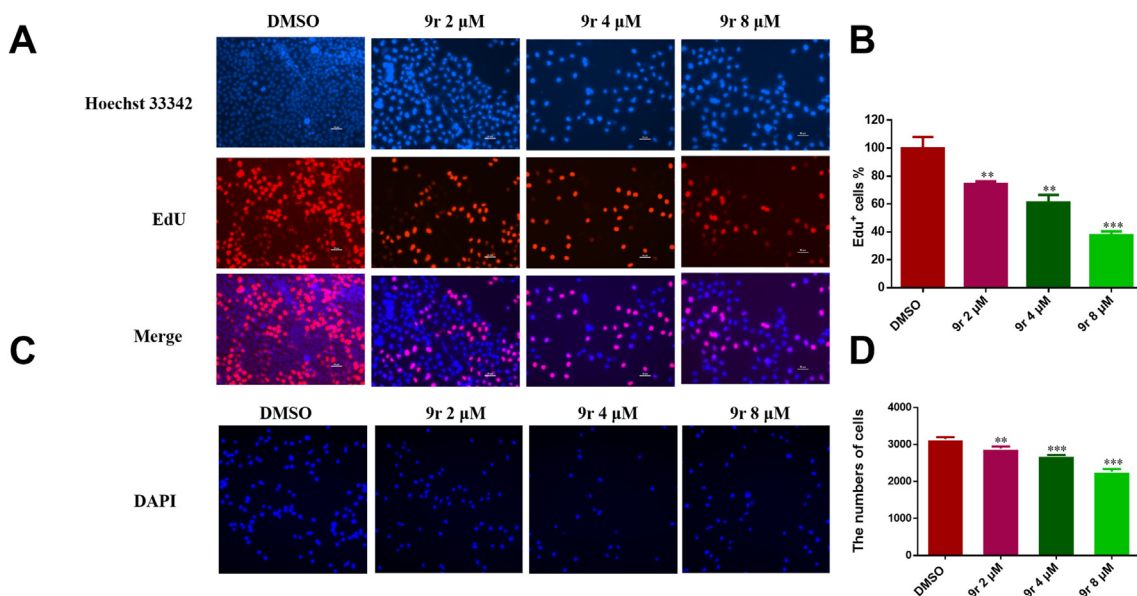


Fig. 7. Effect of compound **9r** on antiproliferation, migration and invasion ability of MGC803 cells. (A, B) Immunofluorescence staining analysis of EDU⁺ and quantification of EDU⁺ in MGC803 cells treated with 0, 2, 4 or 8 μ M of **9r**. (C, D) The migration and invasion ability of MGC803 cells were performed by matrigel-coated transwell assay and analyzed by HCA (ThermoFisher Scientific). Data was shown as mean \pm SD from three independent experiments. * p < 0.05, ** p < 0.01, *** p < 0.001 compared with the control.

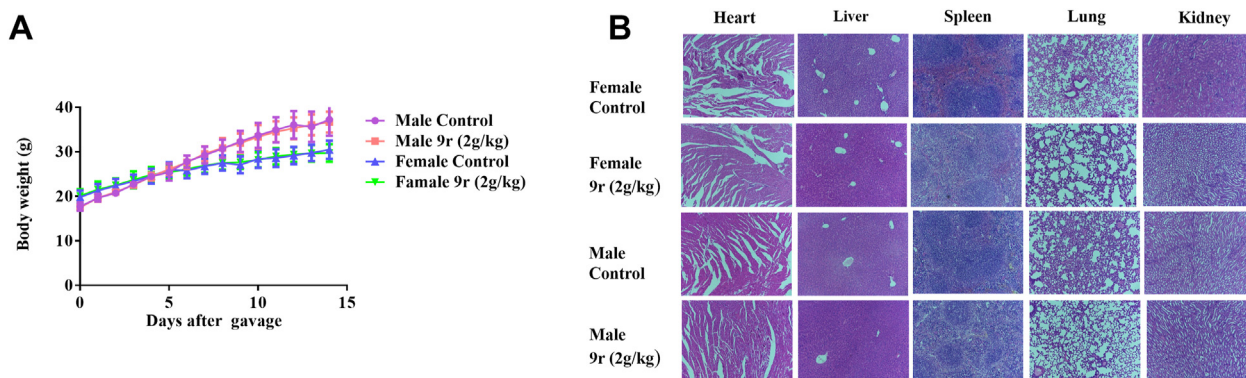


Fig. 8. Acute toxicity in vivo. (A) Body weight was recorded. (B) Heart, liver, spleen, lung and kidney tissue sections were fixed and embedded for HE staining. Data was shown as mean \pm SD from three independent experiments.

4. Experimental section

4.1. General

During the chemical synthesis, all of the solvents and reagents were bought from commercial companies. The chemistry reactions were monitored by TLC and Ultra performance liquid chromatography-mass spectrometry (UPLC-MS, Water, Milford, MA). Column chromatography was performed at medium pressure with silica gel (200–300 mesh). Spectra data of ¹H NMR and ¹³C NMR were obtained on Bruker AVANCE III 400 M spectrometer (Bruker Instruments, Inc.), Chemical shifts (δ) were reported in parts per million (ppm) relative to tetramethylsilane (TMS) and J values were reported in Hertz. The mass spectrum data was recorded by Waters ACQUITY UPLC H-Class ACQUITY QDa (Water, Milford, MA), with electrospray ionization (ESI), C18 column; column size 2.1 mm \times 50 mm; mobile phase 10%–95%, acetonitrile-water-0.1% formic acid served as a binary gradient mobile phase with a flow rate of 0.35 mL/min. High-resolution mass spectra (HR-MS) data were signed by Water Micromass Q-T of Micromass spectrometer with electrospray ionization (Water, Milford, MA).

The melting points of target compounds were tested by WRS-1A digital melting point apparatus. The NMR spectra were shown in Supporting Information.

4.2. General process for the synthesis of the compounds (3a-aq)

To a round-bottom flask (100 mL) was added commercially available phenylhydrazine **1a-p** (10 mmol) and 30 mL ethyl alcohol (20% in water), then stirred at room temperature, followed by adding aromatic aldehyde **2a-ac** in portions. Then, the system was refluxed at 80 $^{\circ}$ C for 6–8 h, monitored by TLC until complete conversion, cooled to room temperature, and filtered, the solid was washed with cold ethyl alcohol (20% in water), dried in oven to produce intermediate hydrazones **3a-aq** with more than 90% yield.

4.3. General process for the synthesis of the compounds (4a-aq)

To a stirred solution of compound **3a-aq** (2.5 mmol) in acetonitrile (15 mL) was added ethanolamine (7.5 mmol), TBHP (7.5 mmol) and I₂ (0.5 mmol) in turn, the system was refluxed at 90 $^{\circ}$ C for 4–5 h. Then monitored by TLC until complete conversion,

cooled to room temperature, and added 10 mL water, followed by extracting with ethyl acetate (15 mL * 3). Then, the organic layer was combined, and washed with saturated sodium chloride solution (25 mL). Finally, the solvent was concentrated, and the precipitate was purified by column chromatography over silica gel to give the compound **4a-aq** with 75%–85% yield.

4.4. General process for the synthesis of the compounds (5a-aq)

Compound **4a-aq** (1 mmol) was dissolved in dichloromethane (8 mL), then kept stirring in an ice-bath, followed by adding Dess-Martin periodinane in portions (1.5 mmol). After stirred at room temperature for 12 h, the system was quenched with a solution of saturated sodium thiosulfate and sodium bicarbonate, followed by extracting with ethyl acetate (15 mL * 3). Then, the organic layer was combined, and washed with saturated sodium chloride solution (25 mL). The organic solvent was removed under vacuum to get compound **5a-aq** used directly for next step without purification.

4.5. General process for the synthesis of the compounds (6a-aq)

Compound **5a-aq** (0.5 mmol) was dissolved in methanol (5 mL), then stirred at room temperature, and added methyl 4-aminobenzoate (0.45 mmol), followed by the addition of catalytic amount of acetic acid (0.05 mmol). After stirred for 0.5 h, the sodium cyanoborohydride (0.55 mmol) was added in portions, then stirred for another 12 h. Water (10 mL) was added to quench the system, and extracted with ethyl acetate (15 mL * 3). Then, the organic layer was combined, and washed with saturated sodium chloride solution (25 mL). Finally, removed the solvent and purified by column chromatography over silica gel to give the compound **6a-aq** with 65%–75% yield.

4.6. General process for the synthesis of the compounds (7a)

To a mixture of compound **6a** (0.5 mmol) in methanol (8 mmol) was added sodium hydroxide (2.5 mmol), the system was kept refluxing at 70 °C for 5–6 h, then monitored by TLC until complete conversion, then cooled to room temperature, and the solvent was removed under reduced pressure. Subsequently, the precipitate was dissolved in water (5 mL), followed by adding formic acid to adjust pH to 5–6, the solid was filtered, and washed with water, dried in oven to get compound **7a** as white solid with 95% yield.

4-(((1,3-diphenyl-1H-1,2,4-triazol-5-yl)methyl)amino)benzoic acid (**7a**).

White solid, yield: 68.8%. Mp: 188–189 °C. ¹H NMR (400 MHz, DMSO-*d*₆, ppm) δ 12.08 (s, 1H, OH, D₂O exchangeable), 8.06 (d, *J* = 7.9 Hz, 2H, Ar–H), 7.73–7.68 (m, 3H, Ar–H), 7.66 (s, 1H, Ar–H), 7.62 (d, *J* = 7.6 Hz, 1H, Ar–H), 7.60–7.53 (m, 2H, Ar–H), 7.50 (t, *J* = 7.0 Hz, 2H, Ar–H), 7.45 (dd, *J* = 10.4, 3.8 Hz, 1H, Ar–H), 7.01 (t, *J* = 5.3 Hz, 1H, NH, D₂O exchangeable), 6.61 (d, *J* = 8.4 Hz, 2H, Ar–H), 4.57 (d, *J* = 5.3 Hz, 2H, –CH₂–). ¹³C NMR (101 MHz, DMSO-*d*₆, ppm) δ 167.35, 160.39, 154.14, 151.65, 136.88, 130.98, 130.42, 129.54, 129.43, 129.08, 125.88, 124.69, 38.73. HR-MS(ESI), calcd. C₂₂H₁₈N₄O₂, [M+H]⁺ *m/z*: 371.1508, found: 371.1502.

4.7. General process for the synthesis of the compounds (1, 8a-c)

To a mixture of compound **7a** (0.3 mmol) in dichloromethane (10 mL) was added EDCI (0.9 mmol) and HOBt (0.3 mmol), then stirred at room temperature for 0.5 h. Subsequently, *tert*-Butyl carbazate (0.6 mmol), one of involved amine fragments, was added. The system was kept stirring at room temperature for another 12 h.

Then water (10 mL) was added to quench the system, and extracted with dichloromethane (15 mL * 3). Next, the organic layer was combined, and washed with saturated sodium chloride solution (25 mL). Finally, the solvent was concentrated and purified by column chromatography over silica gel to get the Boc-protected amide product, then this solid was dissolved into 1,4-dioxane, followed by the addition of trifluoroacetic acid (TFA) to remove the Boc protecting group. When complete conversion, the solvent was removed under reduced pressure to get compound **1** as white solid. Likewise, *tert*-Butyl carbamate, methylamine hydrochloride, and *N*-(*tert*-Butoxycarbonyl)-1,2-phenylenediamine was used to produce compounds **8a-c**, respectively, the yield ranged from 60% to 65%.

4.7.1. 4-(((1,3-diphenyl-1H-1,2,4-triazol-5-yl)methyl)amino)benzohydrazide (**1**)

White solid, yield: 70%. Mp: 191–192 °C. ¹H NMR (400 MHz, DMSO-*d*₆, ppm) δ 9.34 (s, 1H, NH, D₂O exchangeable), 8.06 (d, *J* = 6.9 Hz, 2H, Ar–H), 7.70 (d, *J* = 7.6 Hz, 2H, Ar–H), 7.61 (dd, *J* = 9.5, 5.1 Hz, 3H, Ar–H), 7.56 (d, *J* = 10.2 Hz, 2H, Ar–H), 7.48 (dt, *J* = 6.9, 4.8 Hz, 3H, Ar–H), 6.75 (t, *J* = 5.5 Hz, 1H, NH, D₂O exchangeable), 6.58 (d, *J* = 8.6 Hz, 2H, Ar–H), 4.54 (d, *J* = 5.5 Hz, 2H, –CH₂–), 4.32 (s, 2H, NH₂, D₂O exchangeable). ¹³C NMR (101 MHz, DMSO-*d*₆, ppm) δ 166.19, 160.35, 154.33, 150.24, 136.90, 130.41, 129.54, 129.44, 129.06, 128.81, 128.26, 125.87, 124.63, 120.94, 111.22. HR-MS(ESI), calcd. C₂₂H₂₀N₆O, [M + H]⁺ *m/z*: 385.1777, found: 385.1770.

4.7.2. 4-(((1,3-diphenyl-1H-1,2,4-triazol-5-yl)methyl)amino)benzamide (**8a**)

White solid, yield: 68%. Mp: 220–221 °C. ¹H NMR (400 MHz, DMSO-*d*₆, ppm) δ 8.08–8.04 (m, 2H, Ar–H), 7.70 (d, *J* = 7.4 Hz, 2H, Ar–H), 7.62 (dd, *J* = 7.7, 4.2 Hz, 3H, Ar–H), 7.57 (dd, *J* = 10.2, 5.4 Hz, 2H, Ar–H), 7.52–7.41 (m, 3H, Ar–H), 6.90 (s, 1H, NH, D₂O exchangeable), 6.75 (s, 1H, NH, D₂O exchangeable), 6.58 (d, *J* = 8.6 Hz, 2H), 4.54 (d, *J* = 4.9 Hz, 2H, –CH₂–). ¹³C NMR (101 MHz, DMSO-*d*₆, ppm) δ 167.83, 160.36, 154.35, 150.35, 136.91, 130.44, 129.53, 129.43, 129.05, 128.93, 128.81, 125.87, 124.63, 121.99, 111.09, 38.87. HR-MS(ESI), calcd. C₂₂H₁₉N₅O, [M + H]⁺ *m/z*: 370.1668, found: 370.1662.

4.7.3. 4-(((1,3-diphenyl-1H-1,2,4-triazol-5-yl)methyl)amino)-*N*-methylbenzamide (**8b**)

White solid, yield: 75%. Mp: 221–222 °C. ¹H NMR (400 MHz, DMSO-*d*₆, ppm) δ 8.08–8.04 (m, 2H, Ar–H), 8.00 (d, *J* = 4.5 Hz, 1H, NH, D₂O exchangeable), 7.70 (d, *J* = 7.6 Hz, 2H, Ar–H), 7.64–7.54 (m, 5H, Ar–H), 7.53–7.42 (m, 3H, Ar–H), 6.73 (t, *J* = 5.5 Hz, 1H, NH, D₂O exchangeable), 6.58 (d, *J* = 8.7 Hz, 2H), 4.54 (d, *J* = 5.5 Hz, 2H, –CH₂–), 2.71 (d, *J* = 4.5 Hz, 3H, –CH₃–). ¹³C NMR (101 MHz, DMSO-*d*₆, ppm) δ 166.51, 160.35, 154.36, 150.16, 136.92, 130.44, 129.53, 129.43, 129.05, 128.80, 128.35, 125.86, 124.64, 122.35, 111.17, 38.87, 26.05. HR-MS(ESI), calcd. C₂₃H₂₁N₅O, [M + H]⁺ *m/z*: 384.1824, found: 384.1818.

4.7.4. *N*-(2-aminophenyl)-4-(((1,3-diphenyl-1H-1,2,4-triazol-5-yl)methyl)amino)benzamide (**8c**)

White solid, yield: 63%. Mp: 240–241 °C. ¹H NMR (400 MHz, DMSO-*d*₆, ppm) δ 9.29 (s, 1H, NH, D₂O exchangeable), 8.27–7.99 (m, 2H, Ar–H), 7.75 (d, *J* = 8.7 Hz, 2H, Ar–H), 7.73–7.69 (m, 2H, Ar–H), 7.62 (t, *J* = 7.4 Hz, 2H, Ar–H), 7.57 (d, *J* = 7.2 Hz, 1H, Ar–H), 7.50 (s, 1H, Ar–H), 7.49–7.41 (m, 2H, Ar–H), 7.13 (dd, *J* = 7.8, 1.2 Hz, 1H, Ar–H), 6.94 (dd, *J* = 10.9, 4.4 Hz, 1H, Ar–H), 6.85 (t, *J* = 5.5 Hz, 1H, NH, D₂O exchangeable), 6.76 (dd, *J* = 7.9, 1.2 Hz, 1H, Ar–H), 6.63 (d, *J* = 8.8 Hz, 2H, Ar–H), 6.61–6.55 (m, 1H, Ar–H), 4.81 (s, 2H, NH, D₂O exchangeable), 4.58 (d, *J* = 5.6 Hz, 2H, –CH₂–). ¹³C NMR (101 MHz, DMSO-*d*₆, ppm) δ 164.96, 160.38, 154.35, 150.56, 142.94,

136.92, 130.44, 129.56, 129.21, 125.87, 124.64, 124.05, 116.30, 116.16, 111.17. HR-MS(ESI), calcd. $C_{28}H_{24}N_6O$, $[M + H]^+$ m/z : 461.2090, found: 461.2083.

4.8. General process for the synthesis of the compounds (9a-aq)

To a mixture of compound **6a-aq** (0.25 mmol) in DCM: MeOH = 1:2 (8 mL) was added hydroxylamine (50% in water, 5 mmol), then stirred at room temperature for 0.5 h, followed by adding sodium hydroxide (1 mmol). The system was kept stirring for another 0.5–1 h, monitored by TLC until complete conversion. Then the solvent was removed under vacuum, and the precipitate was dissolved in water (5 mL), followed by the addition of formic acid to adjust pH to 5–6, the solid was filtered, and washed with water, dried in oven to get target compounds **9a-9aq** with 75%–85% yield.

4.8.1. 4-(((1,3-diphenyl-1H-1,2,4-triazol-5-yl)methyl)amino)-N-hydroxybenzamide (9a)

White solid, yield: 85%. Mp: 213–214 °C. 1H NMR (400 MHz, DMSO- d_6 , ppm) δ 10.84 (s, 1H, OH, D₂O exchangeable), 8.78 (s, 1H, NH, D₂O exchangeable), 8.05 (d, J = 7.5 Hz, 2H, Ar–H), 7.69 (d, J = 7.8 Hz, 2H, Ar–H), 7.61 (td, J = 14.5, 13.6, 6.3 Hz, 4H, Ar–H), 7.50 (h, J = 7.7, 6.9 Hz, 4H, Ar–H), 6.76 (t, J = 5.7 Hz, 1H, NH, D₂O exchangeable), 6.59 (t, J = 7.9 Hz, 2H, Ar–H), 4.55 (dd, J = 9.5, 5.5 Hz, 2H, –CH₂–). ^{13}C NMR (101 MHz, DMSO- d_6 , ppm) δ 160.33, 154.30, 154.15, 150.28, 136.82, 130.95, 130.32, 129.54, 129.47, 129.09, 128.82, 128.15, 125.85, 124.67, 124.61, 120.15, 111.26. HR-MS (ESI), calcd. $C_{22}H_{19}N_5O_2$, $[M+H]^+$ m/z : 386.1617, found: 386.1610.

4.8.2. N-hydroxy-4-(((1-phenyl-3-(o-tolyl)-1H-1,2,4-triazol-5-yl)methyl)amino)benzamide (9b)

Off-white solid, yield: 81%. Mp: 224–225 °C. 1H NMR (400 MHz, DMSO- d_6 , ppm) δ 10.80 (s, 1H, OH, D₂O exchangeable), 8.71 (s, 1H, NH, D₂O exchangeable), 7.97 (d, J = 7.0 Hz, 1H, Ar–H), 7.71 (d, J = 7.6 Hz, 2H, Ar–H), 7.61 (t, J = 7.5 Hz, 2H, Ar–H), 7.54 (dd, J = 12.0, 8.0 Hz, 3H, Ar–H), 7.37–7.26 (m, 3H, Ar–H), 6.74 (t, J = 5.5 Hz, 1H, NH, D₂O exchangeable), 6.62 (d, J = 8.7 Hz, 2H, Ar–H), 4.56 (d, J = 5.5 Hz, 2H, –CH₂–), 2.61 (s, 3H, –CH₃). ^{13}C NMR (101 MHz, DMSO- d_6 , ppm) δ 161.12, 153.29, 150.40, 136.99, 136.39, 131.23, 129.55, 128.94, 128.13, 125.84, 124.41, 120.27, 111.36, 21.66. HR-MS (ESI), calcd. $C_{23}H_{21}N_5O_2$, $[M+H]^+$ m/z : 400.1773, found: 400.1767.

4.8.3. N-hydroxy-4-(((1-phenyl-3-(p-tolyl)-1H-1,2,4-triazol-5-yl)methyl)amino)benzamide (9c)

Brown solid, yield: 82%. Mp: 224–225 °C. 1H NMR (400 MHz, DMSO- d_6 , ppm) δ 7.92–7.81 (m, 2H, Ar–H), 7.68 (d, J = 7.9 Hz, 2H, Ar–H), 7.65–7.48 (m, 5H, Ar–H), 7.38 (t, J = 7.6 Hz, 1H, Ar–H), 7.27 (d, J = 7.7 Hz, 1H, Ar–H), 6.75 (t, J = 5.7 Hz, 1H, NH, D₂O exchangeable), 6.55 (dd, J = 11.3, 8.4 Hz, 2H, Ar–H), 4.53 (d, J = 5.5 Hz, 2H, –CH₂–), 2.38 (s, 3H, –CH₃). ^{13}C NMR (101 MHz, DMSO- d_6 , ppm) δ 160.41, 154.20, 150.25, 137.99, 136.83, 130.76, 130.26, 130.11, 129.53, 129.06, 128.73, 128.13, 126.33, 124.58, 123.05, 120.16, 111.25, 20.96. HR-MS (ESI), calcd. $C_{23}H_{21}N_5O_2$, $[M+H]^+$ m/z : 400.1773, found: 400.1767.

4.8.4. N-hydroxy-4-(((1-phenyl-3-(p-tolyl)-1H-1,2,4-triazol-5-yl)methyl)amino)benzamide (9d)

Light yellow solid, yield: 83%. Mp: 224–225 °C. 1H NMR (400 MHz, DMSO- d_6 , ppm) δ 10.85 (s, 1H, OH, D₂O exchangeable), 8.80 (s, 1H, NH, D₂O exchangeable), 7.95 (d, J = 7.9 Hz, 2H, Ar–H), 7.68 (d, J = 7.6 Hz, 2H, Ar–H), 7.64–7.48 (m, 5H, Ar–H), 7.30 (d, J = 8.0 Hz, 2H, Ar–H), 6.75 (t, J = 5.6 Hz, 1H), 6.58 (d, J = 8.6 Hz, 2H, Ar–H), 4.53 (d, J = 5.8 Hz, 2H, –CH₂–), 2.36 (s, 3H, –CH₃). ^{13}C NMR (101 MHz, DMSO- d_6 , ppm) δ 164.79, 160.42, 154.12, 150.28, 138.99,

136.85, 129.52, 129.37, 129.02, 128.15, 127.61, 125.82, 124.58, 120.14, 111.26, 20.91. HR-MS (ESI), calcd. $C_{23}H_{21}N_5O_2$, $[M+H]^+$ m/z : 400.1773, found: 400.1767.

4.8.5. 4-(((3-(4-ethylphenyl)-1-phenyl-1H-1,2,4-triazol-5-yl)methyl)amino)-N-hydroxybenzamide (9e)

Dark yellow solid, yield: 81%. Mp: 227–228 °C. 1H NMR (400 MHz, DMSO- d_6 , ppm) δ 10.84 (s, 1H, OH, D₂O exchangeable), 8.78 (s, 1H, NH, D₂O exchangeable), 7.97 (d, J = 8.0 Hz, 2H, Ar–H), 7.68 (d, J = 7.8 Hz, 2H, Ar–H), 7.66–7.48 (m, 5H, Ar–H), 7.33 (d, J = 8.0 Hz, 2H, Ar–H), 6.75 (t, J = 5.6 Hz, 1H, NH, D₂O exchangeable), 6.58 (t, J = 7.3 Hz, 2H, Ar–H), 4.54 (dd, J = 9.0, 5.4 Hz, 2H, –CH₂–), 2.66 (q, J = 7.6 Hz, 2H, –CH₂–), 1.21 (t, J = 7.6 Hz, 3H, –CH₃). ^{13}C NMR (101 MHz, DMSO- d_6 , ppm) δ 160.42, 154.12, 150.28, 145.21, 136.85, 130.93, 129.52, 129.01, 128.17, 127.86, 125.91, 124.62, 124.57, 120.14, 111.26, 27.97, 15.30. LC-MS t_R = 4.748 min; calcd. $C_{24}H_{23}N_5O_2$, $[M+H]^+$ m/z : 414.20, found: 414.23.

4.8.6. N-hydroxy-4-(((3-(4-isopropylphenyl)-1-phenyl-1H-1,2,4-triazol-5-yl)methyl)amino)benzamide (9f)

Yellowish brown solid, yield: 86%. Mp: 227–228 °C. 1H NMR (400 MHz, DMSO- d_6 , ppm) δ 7.97 (d, J = 8.0 Hz, 2H, Ar–H), 7.68 (d, J = 7.3 Hz, 3H, Ar–H), 7.65–7.47 (m, 4H, Ar–H), 7.36 (d, J = 7.9 Hz, 2H, Ar–H), 6.74 (t, J = 5.6 Hz, 1H, OH, D₂O exchangeable), 6.55 (dd, J = 15.3, 8.3 Hz, 2H, Ar–H), 4.52 (t, J = 4.6 Hz, 2H, –CH₂–), 2.94 (h, J = 7.0 Hz, 1H, –CH–), 1.23 (d, J = 6.8 Hz, 6H, –CH₃). ^{13}C NMR (101 MHz, DMSO- d_6 , ppm) δ 160.41, 154.20, 154.13, 150.26, 149.80, 136.87, 129.52, 129.01, 128.10, 128.01, 126.71, 125.94, 124.56, 111.27, 33.25, 23.67. LC-MS t_R = 5.000 min; calcd. $C_{25}H_{25}N_5O_2$, $[M+H]^+$ m/z : 428.21, found: 428.23.

4.8.7. N-hydroxy-4-(((3-(4-methoxyphenyl)-1-phenyl-1H-1,2,4-triazol-5-yl)methyl)amino)benzamide (9g)

Light yellow solid, yield: 81%. Mp: 210–211 °C. 1H NMR (400 MHz, DMSO- d_6 , ppm) δ 10.80 (s, 1H, OH, D₂O exchangeable), 8.71 (s, 1H, NH, D₂O exchangeable), 7.98 (d, J = 8.4 Hz, 2H, Ar–H), 7.68 (d, J = 7.4 Hz, 2H, Ar–H), 7.59 (t, J = 7.2 Hz, 2H, Ar–H), 7.52 (d, J = 8.5 Hz, 3H), 7.04 (d, J = 8.4 Hz, 2H, Ar–H), 6.75 (s, 1H, NH, D₂O exchangeable), 6.58 (d, J = 8.4 Hz, 2H, Ar–H), 4.51 (d, J = 4.5 Hz, 2H, –CH₂–), 3.80 (s, 3H, –CH₃). ^{13}C NMR (101 MHz, DMSO) δ 164.77, 160.30, 160.20, 154.03, 150.33, 136.97, 129.51, 128.92, 128.17, 127.38, 124.56, 123.00, 120.26, 114.18, 111.28, 55.18. HR-MS(ESI), calcd. $C_{23}H_{21}N_5O_3$, $[M+H]^+$ m/z : 416.1722, found: 416.1716.

4.8.8. 4-(((3-(4-fluorophenyl)-1-phenyl-1H-1,2,4-triazol-5-yl)methyl)amino)-N-hydroxybenzamide (9h)

Gray solid, yield: 84%. Mp: 214–215 °C. 1H NMR (400 MHz, DMSO- d_6 , ppm) δ 8.09 (dd, J = 8.6, 5.6 Hz, 2H, Ar–H), 7.69 (d, J = 7.6 Hz, 2H, Ar–H), 7.65–7.48 (m, 5H, Ar–H), 7.33 (t, J = 8.7 Hz, 2H, Ar–H), 6.75 (t, J = 5.6 Hz, 1H, NH, D₂O exchangeable), 6.56 (dd, J = 13.2, 8.5 Hz, 2H, Ar–H), 4.53 (d, J = 5.5 Hz, 2H, –CH₂–). ^{13}C NMR (101 MHz, DMSO- d_6 , ppm) δ 164.02, 161.57, 159.56, 154.43, 150.24, 136.75, 130.76, 129.54, 129.13, 128.13, 128.05, 126.91, 124.62, 120.17, 115.93, 115.71, 111.27, 110.97. LC-MS t_R = 4.322 min; calcd. $C_{22}H_{18}FN_5O_2$, $[M+H]^+$ m/z : 404.15, found: 404.15.

4.8.9. 4-(((3-(2-chlorophenyl)-1-phenyl-1H-1,2,4-triazol-5-yl)methyl)amino)-N-hydroxybenzamide (9i)

Gray solid, yield: 81%. Mp: 214–215 °C. 1H NMR (400 MHz, DMSO- d_6 , ppm) δ 10.80 (s, 1H, OH, D₂O exchangeable), 8.70 (s, 1H, NH, D₂O exchangeable), 8.00–7.83 (m, 1H, Ar–H), 7.71 (d, J = 7.7 Hz, 2H, Ar–H), 7.66–7.54 (m, 4H, Ar–H), 7.53–7.44 (m, 4H, Ar–H), 6.74 (s, 1H, NH, D₂O exchangeable), 6.60 (d, J = 8.4 Hz, 2H, Ar–H), 4.57 (s, 2H, –CH₂–). ^{13}C NMR (101 MHz, DMSO- d_6 , ppm) δ 164.74, 158.90, 153.70, 150.34, 136.82, 131.56, 131.27, 130.71, 130.65, 129.56, 129.37,

129.07, 128.13, 127.25, 124.53, 120.30, 111.35. HR-MS (ESI), calcd. $C_{22}H_{18}ClN_5O_2$, $[M+Na]^+$ m/z : 442.1047, found: 442.1040.

4.8.10. 4-(((3-(3-chlorophenyl)-1-phenyl-1H-1,2,4-triazol-5-yl)methyl)amino)-N-hydroxybenzamide (9j)

Brown solid, yield: 83%. Mp: 214–215 °C. 1H NMR (400 MHz, DMSO- d_6 , ppm) δ 10.80 (s, 1H, OH, D₂O exchangeable), 8.71 (s, 1H, NH, D₂O exchangeable), 8.21–7.94 (m, 2H, Ar–H), 7.71 (d, J = 7.2 Hz, 2H, Ar–H), 7.61 (t, J = 7.3 Hz, 2H, Ar–H), 7.57 (d, J = 7.0 Hz, 1H, Ar–H), 7.56–7.52 (m, 3H, Ar–H), 7.51 (s, 1H, Ar–H), 6.75 (t, J = 5.4 Hz, 1H, NH, D₂O exchangeable), 6.58 (d, J = 8.7 Hz, 2H, Ar–H), 4.54 (d, J = 5.5 Hz, 1H, –CH₂–). ^{13}C NMR (101 MHz, DMSO- d_6 , ppm) δ 164.72, 159.07, 154.70, 150.26, 136.75, 133.60, 132.44, 130.95, 129.56, 129.30, 129.22, 128.17, 125.36, 124.67, 124.42, 120.33, 111.28. HR-MS (ESI), calcd. $C_{22}H_{18}ClN_5O_2$, $[M+Na]^+$ m/z : 442.1047, found: 442.1040.

4.8.11. 4-(((3-(4-chlorophenyl)-1-phenyl-1H-1,2,4-triazol-5-yl)methyl)amino)-N-hydroxybenzamide (9k)

Dark brown solid, yield: 82%. Mp: 214–215 °C. 1H NMR (400 MHz, DMSO- d_6 , ppm) δ 10.79 (s, 1H, OH, D₂O exchangeable), 8.70 (s, 1H, NH, D₂O exchangeable), 8.05 (d, J = 8.2 Hz, 2H, Ar–H), 7.69 (d, J = 7.7 Hz, 2H, Ar–H), 7.61 (t, J = 7.3 Hz, 2H, Ar–H), 7.58–7.54 (m, 3H, Ar–H), 7.51 (d, J = 8.3 Hz, 2H, Ar–H), 6.74 (d, J = 5.9 Hz, 1H, NH, D₂O exchangeable), 6.57 (d, J = 8.4 Hz, 2H, Ar–H), 4.53 (d, J = 5.4 Hz, 2H, –CH₂–). ^{13}C NMR (101 MHz, DMSO- d_6 , ppm) δ 164.75, 159.44, 154.59, 150.29, 136.80, 134.05, 129.55, 129.29, 129.15, 128.96, 128.17, 127.60, 124.65, 120.30, 111.28. HR-MS (ESI), calcd. $C_{22}H_{18}ClN_5O_2$, $[M+Na]^+$ m/z : 442.1047, found: 420.1040.

4.8.12. 4-(((3-(3,4-dichlorophenyl)-1-phenyl-1H-1,2,4-triazol-5-yl)methyl)amino)-N-hydroxybenzamide (9l)

Gray solid, yield: 81%. Mp: 214–215 °C. 1H NMR (400 MHz, DMSO- d_6 , ppm) δ 10.80 (s, 1H, OH, D₂O exchangeable), 8.71 (s, 1H, NH, D₂O exchangeable), 8.18 (s, 1H, Ar–H), 8.00 (d, J = 8.4 Hz, 1H, Ar–H), 7.77 (d, J = 8.4 Hz, 1H, Ar–H), 7.71 (d, J = 7.8 Hz, 2H, Ar–H), 7.66–7.56 (m, 3H, Ar–H), 7.52 (d, J = 8.4 Hz, 2H, Ar–H), 6.75 (t, J = 5.2 Hz, 1H, NH, D₂O exchangeable), 6.58 (d, J = 8.5 Hz, 2H, Ar–H), 4.54 (d, J = 5.3 Hz, 2H, –CH₂–). ^{13}C NMR (101 MHz, DMSO- d_6 , ppm) δ 164.72, 158.33, 154.91, 150.24, 136.67, 132.01, 131.73, 131.36, 130.96, 129.57, 125.90, 124.68, 120.34, 111.28. HR-MS (ESI), calcd. $C_{22}H_{17}Cl_2N_5O_2$, $[M+Na]^+$ m/z : 476.0657, found: 476.0650.

4.8.13. 4-(((3-(4-bromophenyl)-1-phenyl-1H-1,2,4-triazol-5-yl)methyl)amino)-N-hydroxybenzamide (9m)

White gray solid, yield: 84%. Mp: 214–215 °C. 1H NMR (400 MHz, DMSO- d_6 , ppm) δ 10.80 (s, 1H, OH, D₂O exchangeable), 8.70 (s, 1H, NH, D₂O exchangeable), 7.98 (d, J = 8.2 Hz, 2H, Ar–H), 7.69 (d, J = 8.3 Hz, 4H, Ar–H), 7.60 (t, J = 7.5 Hz, 2H, Ar–H), 7.56 (d, J = 7.0 Hz, 1H, Ar–H), 7.51 (d, J = 8.4 Hz, 2H, Ar–H), 6.75 (s, 1H, NH, D₂O exchangeable), 6.57 (d, J = 8.4 Hz, 2H, Ar–H), 4.52 (d, J = 4.1 Hz, 2H, –CH₂–). ^{13}C NMR (101 MHz, DMSO- d_6 , ppm) δ 164.75, 159.50, 154.61, 150.29, 136.80, 131.88, 129.63, 129.55, 129.16, 128.17, 127.86, 124.65, 122.77, 120.29, 111.27. HR-MS (ESI), calcd. $C_{22}H_{18}BrN_5O_2$, $[M+Na]^+$ m/z : 486.0542, found: 464.0535.

4.8.14. N-hydroxy-4-(((1-phenyl-3-(4-(trifluoromethyl)phenyl)-1H-1,2,4-triazol-5-yl)methyl)amino)benzamide (9n)

Pale pink solid, yield: 85%. Mp: 214–215 °C. 1H NMR (400 MHz, DMSO- d_6 , ppm) δ 10.79 (s, 1H, OH, D₂O exchangeable), 8.70 (s, 1H, NH, D₂O exchangeable), 8.18 (d, J = 2.1 Hz, 1H, Ar–H), 8.00 (dd, J = 8.5, 2.1 Hz, 1H, Ar–H), 7.77 (d, J = 8.4 Hz, 1H, Ar–H), 7.70 (d, J = 7.6 Hz, 2H, Ar–H), 7.62 (d, J = 7.5 Hz, 2H, Ar–H), 7.60–7.54 (m, 2H, Ar–H), 7.51 (d, J = 8.4 Hz, 2H, Ar–H), 6.74 (d, J = 5.7 Hz, 1H, NH,

D₂O exchangeable), 6.56 (d, J = 8.3 Hz, 2H, Ar–H), 4.53 (d, J = 5.5 Hz, 2H, –CH₂–). ^{13}C NMR (101 MHz, DMSO- d_6 , ppm) δ 164.73, 158.33, 154.91, 150.24, 136.67, 132.01, 131.72, 131.35, 130.97, 129.57, 129.29, 128.18, 127.33, 125.90, 124.68, 120.35, 111.29, 38.87. LC-MS t_R = 5.083 min; calcd. $C_{23}H_{18}F_3N_5O_2$, $[M+H]^+$ m/z : 454.15, found: 454.07.

4.8.15. 4-(((3-(benzo[b]thiophen-2-yl)-1-phenyl-1H-1,2,4-triazol-5-yl)methyl)amino)-N-hydroxybenzamide (9o)

Dark brown solid, yield: 84%. Mp: 231–232 °C. 1H NMR (400 MHz, DMSO- d_6 , ppm) δ 10.80 (s, 1H, OH, D₂O exchangeable), 8.71 (s, 1H, NH, D₂O exchangeable), 8.01 (d, J = 6.5 Hz, 2H, Ar–H), 7.93 (s, 1H, Ar–H), 7.71 (d, J = 7.6 Hz, 2H, Ar–H), 7.66–7.55 (m, 3H, Ar–H), 7.52 (d, J = 8.3 Hz, 2H, Ar–H), 7.45–7.38 (m, 2H, Ar–H), 6.79 (s, 1H, NH, D₂O exchangeable), 6.57 (d, J = 8.5 Hz, 2H, Ar–H), 4.54 (d, J = 5.5 Hz, 2H, –CH₂–). ^{13}C NMR (101 MHz, DMSO- d_6 , ppm) δ 164.75, 162.28, 156.74, 154.81, 150.25, 139.56, 139.17, 136.61, 133.06, 129.59, 129.31, 128.20, 125.40, 124.84, 124.80, 124.37, 122.88, 122.61, 120.33, 111.26, 38.78. HR-MS (ESI), calcd. $C_{24}H_{19}N_5O_2S$, $[M+Na]^+$ m/z : 464.1157, found: 464.1150.

4.8.16. N-hydroxy-4-(((3-(3-methylthiophen-2-yl)-1-phenyl-1H-1,2,4-triazol-5-yl)methyl)amino)benzamide (9p)

Gray solid, yield: 81%. Mp: 231–232 °C. 1H NMR (400 MHz, DMSO- d_6 , ppm) δ 10.80 (s, 1H, OH, D₂O exchangeable), 8.71 (s, 1H, NH, D₂O exchangeable), 7.68 (d, J = 7.7 Hz, 2H, Ar–H), 7.60 (t, J = 7.3 Hz, 2H, Ar–H), 7.55 (d, J = 7.0 Hz, 1H, Ar–H), 7.53–7.46 (m, 3H, Ar–H), 7.01 (d, J = 4.8 Hz, 1H, Ar–H), 6.76 (s, 1H, NH, D₂O exchangeable), 6.56 (d, J = 8.3 Hz, 2H, Ar–H), 4.51 (s, 2H, –CH₂–), 2.54 (s, 3H, –CH₃–). ^{13}C NMR (101 MHz, DMSO- d_6 , ppm) δ 164.73, 157.38, 153.59, 150.28, 137.06, 136.79, 131.60, 129.55, 129.04, 128.14, 126.73, 125.91, 124.59, 120.28, 111.28, 38.70, 15.46. HR-MS (ESI), calcd. $C_{21}H_{19}N_5O_2S$, $[M+Na]^+$ m/z : 428.1157, found: 428.1150.

4.8.17. 4-(((3-(3-bromothiophen-2-yl)-1-phenyl-1H-1,2,4-triazol-5-yl)methyl)amino)-N-hydroxybenzamide (9q)

Dark brown solid, yield: 83%. Mp: 231–232 °C. 1H NMR (400 MHz, DMSO- d_6 , ppm) δ 10.79 (s, 1H, OH, D₂O exchangeable), 7.78 (d, J = 1.6 Hz, 1H, NH, D₂O exchangeable), 7.69–7.64 (m, 2H, Ar–H), 7.60 (d, J = 2.0 Hz, 2H, Ar–H), 7.58 (t, J = 3.0 Hz, 2H, Ar–H), 7.51 (s, 1H, Ar–H), 7.49 (s, 1H, Ar–H), 6.74 (s, 1H, NH, D₂O exchangeable), 6.53 (d, J = 8.5 Hz, 2H, Ar–H), 4.50 (s, 2H, –CH₂–). ^{13}C NMR (101 MHz, DMSO- d_6 , ppm) δ 164.73, 155.60, 154.71, 150.17, 136.51, 134.71, 129.57, 129.33, 128.18, 127.89, 125.09, 124.77, 120.34, 111.23, 109.54, 38.72. HR-MS (ESI), calcd. $C_{20}H_{16}BrN_5O_2S$, $[M+Na]^+$ m/z : 492.0106, found: 4692.0099.

4.8.18. N-hydroxy-4-(((3-(5-methylthiophen-2-yl)-1-phenyl-1H-1,2,4-triazol-5-yl)methyl)amino)benzamide (9r)

White yellow solid, yield: 84%. Mp: 231–232 °C. 1H NMR (400 MHz, DMSO- d_6 , ppm) δ 10.79 (s, 1H, OH, D₂O exchangeable), 8.70 (s, 1H, NH, D₂O exchangeable), 7.65 (d, J = 7.3 Hz, 2H, Ar–H), 7.58 (dd, J = 14.5, 6.7 Hz, 3H, Ar–H), 7.50 (d, J = 8.3 Hz, 2H, Ar–H), 7.43 (d, J = 3.2 Hz, 1H, Ar–H), 6.85 (d, J = 3.4 Hz, 1H, Ar–H), 6.75 (t, J = 5.5 Hz, 1H, NH, D₂O exchangeable), 6.53 (d, J = 8.2 Hz, 2H, Ar–H), 4.48 (d, J = 5.2 Hz, 2H, –CH₂–), 2.48 (s, 3H, –CH₃–). ^{13}C NMR (101 MHz, DMSO- d_6 , ppm) δ 164.74, 156.83, 154.15, 150.23, 140.98, 136.68, 130.65, 129.53, 129.08, 128.16, 126.41, 126.29, 124.67, 120.27, 111.22, 38.69, 15.00. HR-MS (ESI), calcd. $C_{21}H_{19}N_5O_2S$, $[M+Na]^+$ m/z : 428.1157, found: 406.1150.

4.8.19. N-hydroxy-4-(((1-(4-hydroxyphenyl)-3-(thiophen-2-yl)-1H-1,2,4-triazol-5-yl)methyl)amino)benzamide (9s)

White solid, yield: 82%. Mp: 231–232 °C. 1H NMR (400 MHz, DMSO- d_6 , ppm) δ 10.79 (s, 1H, OH, D₂O exchangeable), 10.03 (s, 1H,

OH, D₂O exchangeable), 8.71 (s, 1H, NH, D₂O exchangeable), 7.62 (d, $J = 4.3$ Hz, 2H, Ar–H), 7.51 (d, $J = 8.4$ Hz, 2H, Ar–H), 7.44 (d, $J = 8.5$ Hz, 2H, Ar–H), 7.15 (t, $J = 4.3$ Hz, 1H, Ar–H), 6.97–6.89 (m, 2H, Ar–H), 6.74 (t, $J = 5.7$ Hz, 1H, NH, D₂O exchangeable), 6.54 (d, $J = 8.4$ Hz, 2H, Ar–H), 4.42 (d, $J = 5.6$ Hz, 2H, –CH₂–). ¹³C NMR (101 MHz, DMSO-*d*₆, ppm) δ 164.77, 158.09, 156.45, 154.17, 150.26, 133.36, 128.17, 128.06, 128.00, 127.23, 126.50, 125.99, 120.21, 115.78, 111.20, 38.47. HR-MS (ESI), calcd. C₂₀H₁₇N₅O₃S, [M+Na]⁺ m/z : 430.0950, found: 430.0943.

4.8.20. 4-(((3-(5-chlorothiophen-2-yl)-1-phenyl-1H-1,2,4-triazol-5-yl)methyl)amino)-N-hydroxybenzamide (9t)

Off-white solid, yield: 84%. Mp: 236–237 °C. ¹H NMR (400 MHz, DMSO-*d*₆, ppm). δ 10.79 (s, 1H, OH, D₂O exchangeable), 8.70 (s, 1H, NH, D₂O exchangeable), 7.66 (d, $J = 6.9$ Hz, 2H, Ar–H), 7.59 (dd, $J = 16.2, 8.2$ Hz, 3H, Ar–H), 7.50 (d, $J = 7.6$ Hz, 3H, Ar–H), 7.20 (d, $J = 3.5$ Hz, 1H, Ar–H), 6.75 (s, 1H, NH, D₂O exchangeable), 6.53 (d, $J = 8.3$ Hz, 2H, Ar–H), 4.50 (d, $J = 4.8$ Hz, 2H, –CH₂–). ¹³C NMR (101 MHz, DMSO-*d*₆, ppm) δ 165.24, 156.29, 155.15, 150.68, 137.02, 132.53, 130.07, 129.79, 128.67, 128.55, 126.41, 125.28, 120.86, 111.74, 100.00, 39.20. HR-MS (ESI), calcd. C₂₀H₁₆ClN₅O₂S, [M+H]⁺ m/z : 426.0791, found: 426.0785.

4.8.21. N-hydroxy-4-(((1-phenyl-3-(thiophen-3-yl)-1H-1,2,4-triazol-5-yl)methyl)amino)benzamide (9u)

Yellow-white solid, yield: 82%. Mp: 231–232 °C. ¹H NMR (400 MHz, DMSO-*d*₆, ppm). δ 10.79 (s, 1H, OH, D₂O exchangeable), 8.70 (s, 1H, NH, D₂O exchangeable), 8.03 (t, $J = 18.9$ Hz, 1H, Ar–H), 7.67 (d, $J = 6.5$ Hz, 3H, Ar–H), 7.60 (t, $J = 6.8$ Hz, 3H, Ar–H), 7.55 (d, $J = 7.1$ Hz, 1H, Ar–H), 7.51 (d, $J = 8.6$ Hz, 2H, Ar–H), 6.75 (s, 1H, NH, D₂O exchangeable), 6.56 (t, $J = 8.9$ Hz, 2H, Ar–H), 4.51 (s, 2H, –CH₂–). ¹³C NMR (101 MHz, DMSO-*d*₆, ppm) δ 165.27, 158.16, 154.50, 150.78, 137.35, 130.02, 129.52, 128.67, 127.91, 126.36, 125.17, 124.83, 120.79, 111.75, 39.31. HR-MS (ESI), calcd. C₂₀H₁₇N₅O₂S, [M+H]⁺ m/z : 392.1181, found: 392.1175.

4.8.22. 4-(((3-(furan-2-yl)-1-phenyl-1H-1,2,4-triazol-5-yl)methyl)amino)-N-hydroxybenzamide (9v)

Light red solid, yield: 82%. Mp: 236–237 °C. ¹H NMR (400 MHz, DMSO-*d*₆, ppm). δ 10.80 (s, 1H, OH, D₂O exchangeable), 8.72 (s, 1H, NH, D₂O exchangeable), 7.83 (s, 1H, Ar–H), 7.68 (d, $J = 7.7$ Hz, 2H, Ar–H), 7.60 (t, $J = 7.4$ Hz, 2H, Ar–H), 7.56 (d, $J = 7.1$ Hz, 1H, Ar–H), 7.51 (d, $J = 8.6$ Hz, 2H, Ar–H), 7.00 (d, $J = 3.3$ Hz, 1H, Ar–H), 6.76 (t, $J = 5.5$ Hz, 1H, NH, D₂O exchangeable), 6.65 (dd, $J = 3.2, 1.7$ Hz, 1H, Ar–H), 6.55 (d, $J = 8.6$ Hz, 2H, Ar–H), 4.56 (t, $J = 20.4$ Hz, 2H, –CH₂–). ¹³C NMR (101 MHz, DMSO-*d*₆, ppm) δ 154.57, 154.52, 153.48, 150.75, 144.66, 137.23, 130.03, 129.55, 128.66, 125.07, 120.80, 111.75, 111.14, 108.39, 39.27, 13.83. HR-MS (ESI), calcd. C₂₀H₁₇N₅O₃, [M+Na]⁺ m/z : 398.1229, found: 398.1223.

4.8.23. N-hydroxy-4-(((3-(5-methylfuran-2-yl)-1-phenyl-1H-1,2,4-triazol-5-yl)methyl)amino)benzamide (9w)

White solid, yield: 83%. Mp: 236–237 °C. ¹H NMR (400 MHz, DMSO-*d*₆, ppm). δ 10.80 (s, 1H, OH, D₂O exchangeable), 8.72 (s, 1H, NH, D₂O exchangeable), 7.66 (d, $J = 7.4$ Hz, 2H, Ar–H), 7.60 (t, $J = 7.4$ Hz, 2H, Ar–H), 7.55 (d, $J = 7.0$ Hz, 1H, Ar–H), 7.50 (d, $J = 8.5$ Hz, 2H, Ar–H), 6.87 (d, $J = 3.1$ Hz, 1H, Ar–H), 6.75 (t, $J = 5.3$ Hz, 1H, NH, D₂O exchangeable), 6.54 (d, $J = 8.6$ Hz, 2H, Ar–H), 6.25 (d, $J = 2.4$ Hz, 1H, Ar–H), 4.51 (d, $J = 5.5$ Hz, 2H, –CH₂–), 2.35 (s, 3H, –CH₃). ¹³C NMR (101 MHz, DMSO) δ 165.26, 154.76, 154.42, 150.75, 146.22, 144.54, 137.19, 130.05, 129.64, 128.67, 125.13, 120.83, 112.25, 111.76, 110.17, 39.27. HR-MS (ESI), calcd. C₂₁H₁₉N₅O₃, [M+H]⁺ m/z : 390.1566, found: 390.1560.

4.8.24. 4-(((3-(5-bromofuran-2-yl)-1-phenyl-1H-1,2,4-triazol-5-yl)methyl)amino)-N-hydroxybenzamide (9x)

Off-white solid, yield: 82%. Mp: 237–238 °C. ¹H NMR (400 MHz, DMSO-*d*₆, ppm). δ 10.79 (s, 1H, OH, D₂O exchangeable), 8.70 (s, 1H, NH, D₂O exchangeable), 7.67 (d, $J = 7.3$ Hz, 2H, Ar–H), 7.63–7.55 (m, 3H, Ar–H), 7.50 (d, $J = 8.6$ Hz, 2H, Ar–H), 7.04 (d, $J = 3.5$ Hz, 1H, Ar–H), 6.77 (d, $J = 3.5$ Hz, 1H, Ar–H), 6.75 (s, 1H, NH, D₂O exchangeable), 6.53 (d, $J = 8.7$ Hz, 2H, Ar–H), 4.52 (d, $J = 3.7$ Hz, 2H, –CH₂–). ¹³C NMR (101 MHz, DMSO-*d*₆, ppm) δ 165.22, 155.03, 153.48, 150.70, 148.20, 137.06, 130.07, 129.77, 128.68, 125.19, 123.35, 120.87, 114.34, 112.68, 111.75, 39.26. HR-MS (ESI), calcd. C₂₀H₁₆BrN₅O₃, [M+H]⁺ m/z : 454.0515, found: 454.0508.

4.8.25. N-hydroxy-4-(((1-phenyl-3-(pyridin-2-yl)-1H-1,2,4-triazol-5-yl)methyl)amino)benzamide (9y)

Bright yellow solid, yield: 85%. Mp: 210–211 °C. ¹H NMR (400 MHz, DMSO-*d*₆, ppm). δ 10.80 (s, 1H, OH, D₂O exchangeable), 8.71 (s, 1H, NH, D₂O exchangeable), 8.68 (d, $J = 4.4$ Hz, 1H, Ar–H), 8.10 (d, $J = 7.9$ Hz, 1H, Ar–H), 7.98–7.90 (m, 1H, Ar–H), 7.71 (d, $J = 7.4$ Hz, 2H, Ar–H), 7.62 (t, $J = 7.4$ Hz, 2H, Ar–H), 7.57 (d, $J = 7.1$ Hz, 1H, Ar–H), 7.53 (t, $J = 7.4$ Hz, 2H, Ar–H), 7.46 (dd, $J = 6.9, 5.2$ Hz, 1H, Ar–H), 6.77 (t, $J = 5.4$ Hz, 1H, NH, D₂O exchangeable), 6.59 (d, $J = 8.6$ Hz, 2H, Ar–H), 4.57 (d, $J = 5.5$ Hz, 2H, –CH₂–). ¹³C NMR (101 MHz, DMSO-*d*₆, ppm) δ 165.27, 160.93, 155.01, 150.82, 150.18, 149.67, 137.59, 137.38, 130.06, 129.67, 128.67, 125.15, 124.73, 122.21, 120.80, 111.80, 39.38. HR-MS (ESI), calcd. C₂₁H₁₈N₆O₂, [M+H]⁺ m/z : 387.1569, found: 387.1563.

4.8.26. N-hydroxy-4-(((1-phenyl-3-(pyridin-3-yl)-1H-1,2,4-triazol-5-yl)methyl)amino)benzamide (9z)

Dark yellowish white solid, yield: 83%. Mp: 210–211 °C. ¹H NMR (400 MHz, DMSO-*d*₆, ppm). δ 10.80 (s, 1H, OH, D₂O exchangeable), 9.22 (s, 1H, NH, D₂O exchangeable), 8.71 (s, 2H, Ar–H), 8.37 (d, $J = 7.9$ Hz, 1H, Ar–H), 7.71 (d, $J = 7.3$ Hz, 2H, Ar–H), 7.62 (t, $J = 7.3$ Hz, 2H, Ar–H), 7.58 (d, $J = 7.0$ Hz, 1H, Ar–H), 7.53 (dd, $J = 11.0, 7.0$ Hz, 3H, Ar–H), 6.76 (s, 1H, NH, D₂O exchangeable), 6.58 (d, $J = 8.6$ Hz, 2H, Ar–H), 4.55 (d, $J = 3.8$ Hz, 2H, –CH₂–). ¹³C NMR (101 MHz, DMSO-*d*₆, ppm) δ 165.27, 158.76, 155.30, 150.86, 150.77, 147.39, 137.24, 133.78, 130.08, 129.77, 128.68, 126.80, 125.24, 124.53, 120.84, 111.80. HR-MS (ESI), calcd. C₂₁H₁₈N₆O₂, [M+H]⁺ m/z : 387.1569, found: 387.1564.

4.8.27. N-hydroxy-4-(((1-phenyl-3-(pyridin-4-yl)-1H-1,2,4-triazol-5-yl)methyl)amino)benzamide (9aa)

White solid, yield: 83%. Mp: 210–211 °C. ¹H NMR (400 MHz, DMSO-*d*₆, ppm). δ 10.80 (s, 1H, OH, D₂O exchangeable), 8.71 (d, $J = 4.2$ Hz, 1H, NH, D₂O exchangeable), 8.70 (d, $J = 4.2$ Hz, 2H, Ar–H), 7.96 (d, $J = 5.4$ Hz, 2H, Ar–H), 7.71 (d, $J = 7.3$ Hz, 2H, Ar–H), 7.65–7.56 (m, 3H, Ar–H), 7.52 (d, $J = 8.4$ Hz, 2H, Ar–H), 6.76 (t, $J = 5.1$ Hz, 1H, Ar–H), 6.57 (d, $J = 8.5$ Hz, 2H), 4.56 (d, $J = 5.3$ Hz, 2H, –CH₂–). ¹³C NMR (101 MHz, DMSO-*d*₆, ppm) δ 165.25, 158.96, 155.64, 150.98, 150.74, 137.97, 137.17, 130.10, 129.91, 128.68, 125.30, 120.87, 120.52, 111.78. HR-MS (ESI), calcd. C₂₁H₁₈N₆O₂, [M+H]⁺ m/z : 387.1569, found: 387.1563.

4.8.28. N-hydroxy-4-(((1-phenyl-3-(quinolin-6-yl)-1H-1,2,4-triazol-5-yl)methyl)amino)benzamide (9 ab)

Light yellow solid, yield: 85%. Mp: 210–211 °C. ¹H NMR (400 MHz, DMSO-*d*₆, ppm). δ 10.79 (s, 1H, OH, D₂O exchangeable), 8.94 (d, $J = 2.7$ Hz, 1H, NH, D₂O exchangeable), 8.70 (s, 2H, Ar–H), 8.55 (d, $J = 8.5$ Hz, 1H, Ar–H), 8.42 (dd, $J = 8.8, 1.7$ Hz, 1H, Ar–H), 8.13 (d, $J = 8.8$ Hz, 1H, Ar–H), 7.74 (d, $J = 7.5$ Hz, 2H, Ar–H), 7.63 (t, $J = 7.5$ Hz, 2H, Ar–H), 7.59 (dd, $J = 7.5, 3.1$ Hz, 2H, Ar–H), 7.52 (d, $J = 8.6$ Hz, 2H, Ar–H), 6.79 (s, 1H, NH, D₂O exchangeable), 6.60 (d, $J = 8.7$ Hz, 2H, Ar–H), 4.58 (d, $J = 5.2$ Hz, 1H, –CH₂–). ¹³C NMR

(101 MHz, DMSO- d_6 , ppm) δ 159.90, 154.72, 151.14, 150.30, 148.05, 136.86, 136.65, 129.63, 129.57, 129.19, 128.34, 128.21, 127.94, 127.04, 125.30, 124.71, 122.07, 120.30, 111.26, 38.93. HR-MS (ESI), calcd. $C_{25}H_{20}N_6O_2$, [M+H]⁺ m/z : 437.1726, found: 437.1719.

4.8.29. 4-(((1-(4-fluorophenyl)-3-phenyl-1H-1,2,4-triazol-5-yl)methyl)amino)-N-hydroxybenzamide (**9ac**)

Off-white solid, yield: 81%. Mp: 214–215 °C. ¹H NMR (400 MHz, DMSO- d_6 , ppm) δ 10.78 (s, 1H, OH, D₂O exchangeable), 8.69 (s, 1H, NH, D₂O exchangeable), 8.05 (d, J = 7.2 Hz, 2H, Ar–H), 7.74 (dd, J = 8.8, 4.7 Hz, 2H, Ar–H), 7.53 (s, 1H, Ar–H), 7.50 (d, J = 5.8 Hz, 2H, Ar–H), 7.48–7.45 (m, 2H, Ar–H), 7.43 (d, J = 8.4 Hz, 2H, Ar–H), 6.70 (t, J = 5.7 Hz, 1H, NH, D₂O exchangeable), 6.57 (d, J = 8.3 Hz, 2H, Ar–H), 4.53 (d, J = 5.3 Hz, 2H, –CH₂–). ¹³C NMR (101 MHz, DMSO- d_6 , ppm) δ 164.76, 163.09, 160.65, 160.33, 154.54, 150.26, 133.37, 133.34, 130.38, 129.45, 128.80, 128.16, 127.19, 127.10, 125.88, 120.32, 116.50, 116.27, 111.28, 38.83. HR-MS (ESI), calcd. $C_{22}H_{18}FN_5O_2$, [M+H]⁺ m/z : 404.1523, found: 404.1516.

4.8.30. 4-(((1-(2-chlorophenyl)-3-phenyl-1H-1,2,4-triazol-5-yl)methyl)amino)-N-hydroxybenzamide (**9ad**)

White solid, yield: 81%. Mp: 214–215 °C. ¹H NMR (400 MHz, DMSO- d_6 , ppm) δ 10.76 (s, 1H, OH, D₂O exchangeable), 8.67 (s, 1H, NH, D₂O exchangeable), 8.16–7.97 (m, 2H, Ar–H), 7.75 (d, J = 8.1 Hz, 1H, Ar–H), 7.68 (d, J = 7.7 Hz, 1H, Ar–H), 7.62 (d, J = 7.8 Hz, 1H, Ar–H), 7.56 (d, J = 7.6 Hz, 1H, Ar–H), 7.49 (d, J = 1.9 Hz, 2H, Ar–H), 7.47 (s, 3H, Ar–H), 6.63 (s, 1H, NH, D₂O exchangeable), 6.49 (d, J = 8.4 Hz, 2H, Ar–H), 4.39 (s, 2H, –CH₂–). ¹³C NMR (101 MHz, DMSO) δ 164.76, 160.74, 155.84, 150.15, 134.28, 131.91, 130.66, 130.33, 129.47, 128.82, 128.36, 128.10, 125.88, 120.25, 111.15, 38.59. HR-MS (ESI), calcd. $C_{22}H_{18}ClN_5O_2$, [M+Na]⁺ m/z : 442.1047, found: 442.1040.

4.8.31. 4-(((1-(3-chlorophenyl)-3-phenyl-1H-1,2,4-triazol-5-yl)methyl)amino)-N-hydroxybenzamide (**9ae**)

White solid, yield: 84%. Mp: 214–215 °C. ¹H NMR (400 MHz, DMSO- d_6 , ppm) δ 10.81 (s, 1H, OH, D₂O exchangeable), 8.70 (s, 1H, NH, D₂O exchangeable), 8.15–7.95 (m, 2H, Ar–H), 7.82 (s, 1H, Ar–H), 7.70 (s, 1H, Ar–H), 7.63 (d, J = 4.5 Hz, 2H, Ar–H), 7.55 (s, 1H, Ar–H), 7.52 (d, J = 6.7 Hz, 2H, Ar–H), 7.49 (d, J = 2.8 Hz, 2H, Ar–H), 6.73 (t, J = 5.7 Hz, 1H, NH, D₂O exchangeable), 6.61 (d, J = 8.3 Hz, 2H, Ar–H), 4.60 (d, J = 5.4 Hz, 2H, –CH₂–). ¹³C NMR (101 MHz, DMSO- d_6 , ppm) δ 164.76, 160.51, 154.70, 150.26, 138.12, 133.71, 131.13, 130.23, 129.56, 128.98, 128.82, 128.17, 125.95, 124.55, 123.30, 120.37, 111.33, 38.99. HR-MS (ESI), calcd. $C_{22}H_{18}ClN_5O_2$, [M+Na]⁺ m/z : 442.1047, found: 442.1040.

4.8.32. 4-(((1-(4-chlorophenyl)-3-phenyl-1H-1,2,4-triazol-5-yl)methyl)amino)-N-hydroxybenzamide (**9af**)

White solid, yield: 84%. Mp: 214–215 °C. ¹H NMR (400 MHz, DMSO- d_6 , ppm) δ 10.79 (s, 1H, OH, D₂O exchangeable), 8.70 (s, 1H, NH, D₂O exchangeable), 8.09–7.98 (m, 2H, Ar–H), 7.72 (d, J = 8.2 Hz, 2H, Ar–H), 7.66 (d, J = 8.3 Hz, 2H, Ar–H), 7.53 (s, 1H, Ar–H), 7.52–7.48 (m, 2H, Ar–H), 7.47 (d, J = 3.2 Hz, 2H, Ar–H), 6.72 (s, 1H, NH, D₂O exchangeable), 6.60–6.47 (m, 2H, Ar–H), 4.56 (d, J = 5.4 Hz, 2H, –CH₂–). ¹³C NMR (101 MHz, DMSO- d_6 , ppm) δ 164.74, 160.46, 154.59, 150.25, 135.78, 133.46, 130.27, 129.52, 128.83, 128.16, 126.37, 125.91, 120.34, 111.30, 38.94. HR-MS (ESI), calcd. $C_{22}H_{18}ClN_5O_2$, [M+H]⁺ m/z : 442.1047, found: 442.1040.

4.8.33. 4-(((1-(3-chlorophenyl)-3-phenyl-1H-1,2,4-triazol-5-yl)methyl)amino)-N-hydroxybenzamide (**9ag**)

Dark brown solid, yield: 81%. Mp: 214–215 °C. ¹H NMR (400 MHz, DMSO- d_6 , ppm) δ 10.78 (s, 1H, OH, D₂O exchangeable), 8.05 (d, J = 7.2 Hz, 2H, Ar–H), 7.79 (d, J = 8.2 Hz, 2H, Ar–H), 7.65 (d,

J = 8.2 Hz, 2H, Ar–H), 7.53 (s, 1H, Ar–H), 7.50 (d, J = 5.9 Hz, 2H, Ar–H), 7.47 (d, J = 3.0 Hz, 2H, Ar–H), 6.59 (d, J = 8.3 Hz, 2H, Ar–H), 4.56 (s, 2H, –CH₂–). ¹³C NMR (101 MHz, DMSO- d_6 , ppm) δ 164.75, 160.49, 154.57, 150.26, 136.20, 132.45, 130.27, 129.52, 128.82, 128.16, 126.60, 125.92, 121.94, 120.37, 111.33, 38.97. HR-MS (ESI), calcd. $C_{22}H_{18}BrN_5O_2$, [M+Na]⁺ m/z : 486.0542, found: 486.0535.

4.8.34. N-hydroxy-4-(((3-phenyl-1-(4-(trifluoromethyl)phenyl)-1H-1,2,4-triazol-5-yl)methyl)amino)benzamide (**9ah**)

Light brown solid, yield: 82%. Mp: 224–225 °C. ¹H NMR (400 MHz, DMSO- d_6 , ppm) δ 10.79 (s, 1H, OH, D₂O exchangeable), 8.69 (s, 1H, NH, D₂O exchangeable), 8.12–8.01 (m, 2H, Ar–H), 7.95 (d, J = 2.6 Hz, 4H, Ar–H), 7.53 (d, J = 2.4 Hz, 1H, Ar–H), 7.51 (s, 2H, Ar–H), 7.48 (d, J = 2.7 Hz, 2H, Ar–H), 6.73 (t, J = 5.7 Hz, 1H, NH, D₂O exchangeable), 6.60 (d, J = 8.3 Hz, 2H, Ar–H), 4.64 (d, J = 5.4 Hz, 2H, –CH₂–). ¹³C NMR (101 MHz, DMSO) δ 164.74, 160.70, 154.89, 150.24, 140.14, 130.12, 129.65, 128.85, 128.15, 126.72, 125.98, 125.05, 122.47, 120.43, 111.37, 39.19. HR-MS (ESI), calcd. $C_{23}H_{18}F_3N_5O_2$, [M+H]⁺ m/z : 454.1491, found: 454.1484.

4.8.35. N-hydroxy-4-(((3-phenyl-1-(p-tolyl)-1H-1,2,4-triazol-5-yl)methyl)amino)benzamide (**9ai**)

Pink solid, yield: 81%. Mp: 224–225 °C. ¹H NMR (400 MHz, DMSO- d_6 , ppm) δ 10.78 (s, 1H, OH, D₂O exchangeable), 8.69 (s, 1H, NH, D₂O exchangeable), 8.05 (d, J = 7.3 Hz, 2H, Ar–H), 7.59–7.55 (m, 2H, Ar–H), 7.53 (d, J = 2.0 Hz, 1H, Ar–H), 7.52–7.49 (m, 2H, Ar–H), 7.48–7.44 (m, 2H, Ar–H), 7.40 (d, J = 8.0 Hz, 2H, Ar–H), 6.74 (d, J = 6.7 Hz, 1H, NH, D₂O exchangeable), 6.68–6.46 (m, 2H, Ar–H), 4.50 (d, J = 4.2 Hz, 2H, –CH₂–), 2.41 (s, 3H, –CH₃). ¹³C NMR (101 MHz, DMSO- d_6 , ppm) δ 164.79, 160.26, 154.22, 150.34, 138.75, 134.49, 130.52, 129.92, 129.36, 128.78, 128.17, 125.85, 124.52, 120.29, 111.29, 38.81, 20.68. HR-MS (ESI), calcd. $C_{23}H_{21}N_5O_2$, [M+H]⁺ m/z : 400.1773, found: 400.1767.

4.8.36. N-hydroxy-4-(((3-phenyl-1-(o-tolyl)-1H-1,2,4-triazol-5-yl)methyl)amino)benzamide (**9aj**)

White solid, yield: 85%. Mp: 224–225 °C. ¹H NMR (400 MHz, DMSO- d_6 , ppm) δ 10.85 (s, 1H, OH, D₂O exchangeable), 8.79 (s, 1H, NH, D₂O exchangeable), 8.03 (dd, J = 8.1, 1.6 Hz, 2H, Ar–H), 7.51 (s, 2H, Ar–H), 7.49 (d, J = 3.4 Hz, 2H, Ar–H), 7.47 (d, J = 7.3 Hz, 3H, Ar–H), 7.45–7.43 (m, 1H, Ar–H), 7.40 (dd, J = 7.4, 1.8 Hz, 1H, Ar–H), 6.68 (t, J = 5.8 Hz, 1H, NH, D₂O exchangeable), 6.57–6.39 (m, 2H, Ar–H), 4.35 (d, J = 5.7 Hz, 2H, –CH₂–), 2.03 (s, 3H, –CH₃). ¹³C NMR (101 MHz, DMSO- d_6 , ppm) δ 164.74, 160.38, 155.20, 150.26, 135.81, 135.13, 131.19, 130.58, 130.07, 129.35, 128.80, 128.13, 127.18, 126.89, 125.80, 120.05, 111.07, 38.30, 16.95. HR-MS (ESI), calcd. $C_{23}H_{21}N_5O_2$, [M+H]⁺ m/z : 400.1773, found: 400.1767.

4.8.37. N-hydroxy-4-(((3-phenyl-1-(m-tolyl)-1H-1,2,4-triazol-5-yl)methyl)amino)benzamide (**9ak**)

Off-white solid, yield: 83%. Mp: 224–225 °C. ¹H NMR (400 MHz, DMSO- d_6 , ppm) δ 8.05 (dd, J = 8.2, 1.7 Hz, 2H, Ar–H), 7.53 (s, 1H, Ar–H), 7.51 (s, 2H, Ar–H), 7.48 (d, J = 2.4 Hz, 3H, Ar–H), 7.47 (d, J = 1.7 Hz, 2H, Ar–H), 7.35 (s, 1H, Ar–H), 6.76 (t, J = 5.6 Hz, 1H, NH, D₂O exchangeable), 6.61–6.55 (m, 2H, Ar–H), 4.53 (d, J = 5.6 Hz, 2H, –CH₂–), 2.38 (s, 3H, –CH₃). ¹³C NMR (101 MHz, DMSO- d_6 , ppm) δ 164.62, 160.27, 154.30, 150.27, 139.29, 136.83, 130.45, 129.64, 129.40, 129.27, 128.80, 128.13, 125.85, 125.10, 121.62, 120.31, 111.27, 38.84, 20.80. HR-MS (ESI), calcd. $C_{23}H_{21}N_5O_2$, [M+H]⁺ m/z : 400.1773, found: 400.1767.

4.8.38. N-hydroxy-4-(((1-(4-methoxyphenyl)-3-phenyl-1H-1,2,4-triazol-5-yl)methyl)amino)benzamide (**9al**)

Flesh red solid, yield: 84%. Mp: 210–211 °C. ¹H NMR (400 MHz, DMSO- d_6 , ppm) δ 10.81 (s, 1H, OH, D₂O exchangeable), 8.72 (s, 1H,

NH, D₂O exchangeable), 8.11–7.94 (m, 2H, Ar–H), 7.62–7.58 (m, 2H, Ar–H), 7.53 (s, 1H, Ar–H), 7.51 (s, 1H, Ar–H), 7.48 (d, *J* = 2.0 Hz, 1H, Ar–H), 7.47–7.40 (m, 2H, Ar–H), 7.18–7.05 (m, 2H, Ar–H), 6.75 (t, *J* = 5.6 Hz, 1H, NH, D₂O exchangeable), 6.57 (d, *J* = 8.5 Hz, 2H, Ar–H), 4.47 (d, *J* = 5.5 Hz, 2H, –CH₂–), 3.84 (s, 3H, –CH₃). ¹³C NMR (101 MHz, DMSO-*d*₆, ppm) δ 164.77, 160.11, 159.51, 154.25, 150.33, 130.55, 129.78, 129.33, 128.78, 128.17, 126.33, 125.81, 120.20, 114.56, 111.25, 55.53, 38.67. HR-MS (ESI), calcd. C₂₃H₂₁N₅O₃, [M+H]⁺ *m/z*: 416.1772, found: 416.1716.

4.8.39. *N*-hydroxy-4-(((3-(4-hydroxyphenyl)-1-(4-methoxyphenyl)-1*H*-1,2,4-triazol-5-yl)methyl)amino)benzamide (9am)

Orange-red solid, yield: 81%. Mp: 210–211 °C. ¹H NMR (400 MHz, DMSO-*d*₆, ppm) δ 10.79 (s, 1H, OH, D₂O exchangeable), 10.01 (s, 1H, OH, D₂O exchangeable), 8.70 (s, 1H, NH, D₂O exchangeable), 8.01–7.84 (m, 2H, Ar–H), 7.53–7.49 (m, 2H, Ar–H), 7.46–7.42 (m, 2H, Ar–H), 7.28 (d, *J* = 7.8 Hz, 2H, Ar–H), 6.96–6.84 (m, 2H, Ar–H), 6.71 (s, 1H, NH, D₂O exchangeable), 6.57 (d, *J* = 8.3 Hz, 2H, Ar–H), 4.48 (dd, *J* = 48.9, 5.5 Hz, 2H, –CH₂–), 2.34 (s, 3H, –OCH₃). ¹³C NMR (101 MHz, DMSO-*d*₆, ppm) δ 164.78, 160.05, 157.97, 153.98, 150.35, 138.71, 129.32, 128.37, 128.16, 127.93, 126.39, 125.74, 120.16, 115.75, 111.23, 38.60, 20.92. LC-MS *t*_R = 4.229 min; calcd. C₂₃H₂₁N₅O₃, [M+H]⁺ *m/z*: 416.18, found: 416.21.

4.8.40. 4-(((1-(3,5-dimethylphenyl)-3-phenyl-1*H*-1,2,4-triazol-5-yl)methyl)amino)-*N*-hydroxybenzamide (9an)

White solid, yield: 82%. Mp: 227–228 °C. ¹H NMR (400 MHz, DMSO-*d*₆, ppm) δ 10.82 (s, 1H, OH, D₂O exchangeable), 8.74 (s, 1H, NH, D₂O exchangeable), 8.03 (dd, *J* = 8.2, 1.5 Hz, 2H, Ar–H), 7.52 (s, 1H, Ar–H), 7.51–7.46 (m, 3H, Ar–H), 7.44 (d, *J* = 6.8 Hz, 1H, Ar–H), 7.26 (s, 2H, Ar–H), 7.16 (s, 1H, Ar–H), 6.74 (t, *J* = 5.5 Hz, 1H, NH, D₂O exchangeable), 6.57 (d, *J* = 8.4 Hz, 2H), 4.52 (d, *J* = 5.6 Hz, 2H, –CH₂–), 2.33 (s, 6H, –CH₃). ¹³C NMR (101 MHz, DMSO-*d*₆, ppm) δ 164.79, 160.19, 154.26, 150.32, 138.97, 136.73, 130.44, 130.36, 129.39, 128.80, 128.15, 125.84, 122.17, 120.14, 111.29, 38.76, 20.71. HR-MS (ESI), calcd. C₂₄H₂₃N₅O₂, [M+H]⁺ *m/z*: 414.1930, found: 414.1923.

4.8.41. 4-(((1-(3,4-dimethylphenyl)-3-phenyl-1*H*-1,2,4-triazol-5-yl)methyl)amino)-*N*-hydroxybenzamide (9ao)

Light red solid, yield: 83%. Mp: 227–228 °C. ¹H NMR (400 MHz, DMSO-*d*₆, ppm) δ 8.13–7.98 (m, 2H, Ar–H), 7.53 (s, 1H, Ar–H), 7.50 (dd, *J* = 8.6, 2.2 Hz, 3H, Ar–H), 7.46 (d, *J* = 5.0 Hz, 2H, Ar–H), 7.44 (d, *J* = 2.4 Hz, 1H, Ar–H), 7.35 (d, *J* = 3.7 Hz, 1H, Ar–H), 6.76 (t, *J* = 5.6 Hz, 1H, NH, D₂O exchangeable), 6.58 (d, *J* = 8.5 Hz, 2H, Ar–H), 4.50 (d, *J* = 5.6 Hz, 2H, –CH₂–), 2.30 (d, *J* = 7.1 Hz, 6H, –CH₃). ¹³C NMR (101 MHz, DMSO-*d*₆, ppm) δ 164.68, 160.16, 154.18, 150.30, 137.82, 137.52, 134.60, 130.49, 130.21, 129.36, 128.79, 128.13, 125.82, 125.49, 121.85, 120.22, 111.28, 38.78, 19.29, 19.04. HR-MS (ESI), calcd. C₂₄H₂₃N₅O₂, [M+H]⁺ *m/z*: 414.1930, found: 414.1923.

4.8.42. 4-(((1-(4-ethylphenyl)-3-phenyl-1*H*-1,2,4-triazol-5-yl)methyl)amino)-*N*-hydroxybenzamide (9ap)

Light yellow solid, yield: 84%. Mp: 227–228 °C. ¹H NMR (400 MHz, DMSO-*d*₆, ppm) δ 10.79 (s, 1H, OH, D₂O exchangeable), 8.70 (d, *J* = 3.9 Hz, 1H, NH, D₂O exchangeable), 8.13–7.86 (m, 2H, Ar–H), 7.59 (d, *J* = 7.8 Hz, 2H, Ar–H), 7.51 (dd, *J* = 5.3, 3.3 Hz, 2H, Ar–H), 7.50–7.45 (m, 2H, Ar–H), 7.43 (d, *J* = 8.0 Hz, 3H, Ar–H), 6.75 (dd, *J* = 7.6, 4.8 Hz, 1H, NH, D₂O exchangeable), 6.59 (dd, *J* = 8.8, 2.8 Hz, 2H, Ar–H), 4.50 (d, *J* = 5.4 Hz, 2H, –CH₂–), 2.71 (q, *J* = 7.6 Hz, 2H, –CH₂–), 1.23 (t, *J* = 7.6 Hz, 3H, –CH₃). ¹³C NMR (101 MHz, DMSO-*d*₆, ppm) δ 164.76, 160.25, 154.20, 150.34, 144.89, 134.66, 130.50, 129.37, 128.79, 128.77, 128.16, 125.84, 124.59, 120.26, 111.29, 38.87, 27.75, 15.38. HR-MS (ESI), calcd. C₂₄H₂₃N₅O₂, [M+H]⁺ *m/z*: 414.1930, found: 414.1923.

4.8.43. *N*-hydroxy-4-(((1-(4-isopropylphenyl)-3-phenyl-1*H*-1,2,4-triazol-5-yl)methyl)amino)benzamide (9aq)

Off-white solid, yield: 81%. Mp: 227–228 °C. ¹H NMR (400 MHz, DMSO-*d*₆, ppm) δ 10.80 (s, 1H, OH, D₂O exchangeable), 8.70 (s, 1H, NH, D₂O exchangeable), 8.07 (t, *J* = 20.6 Hz, 2H, Ar–H), 7.60 (d, *J* = 8.2 Hz, 2H, Ar–H), 7.52 (d, *J* = 8.6 Hz, 2H, Ar–H), 7.47 (t, *J* = 7.2 Hz, 5H, Ar–H), 6.76 (s, 1H, NH, D₂O exchangeable), 6.59 (d, *J* = 8.6 Hz, 2H, Ar–H), 4.50 (d, *J* = 5.0 Hz, 2H, –CH₂–), 3.00 (dt, *J* = 13.6, 6.7 Hz, 1H, –CH–), 1.26 (d, *J* = 6.9 Hz, 6H, –CH₃). ¹³C NMR (101 MHz, DMSO) δ 164.76, 160.24, 154.17, 150.34, 149.43, 134.72, 130.50, 129.38, 128.80, 128.16, 127.34, 125.83, 124.59, 120.25, 111.30, 38.86, 33.12, 23.71. HR-MS (ESI), calcd. C₂₅H₂₅N₅O₂, [M+H]⁺ *m/z*: 428.2086, found: 428.2080.

4.9. Cell line and reagents

Human gastric cancer cell line (MGC803), obtained from the Cell Bank of Shanghai, was grown in Dulbecco's modified eagle medium (DMEM, Gibco, US), supplemented with penicillin G (100 UI/mL), streptomycin (100 mg/mL) and 10% fetal calf serum at 37 °C in 5% CO₂ atmosphere.

4.10. Cell viability

For cell viability of compounds, MGC803 was seeded at a density of 2500 cells per well in 96-well plate at 37 °C in 5% CO₂ atmosphere. Cells were then allowed to adhere for 24 h, medium in the wells was replaced with fresh medium containing compound which was diluted in 7 dilution steps covering the range from 50 μ M to 0.78 μ M. And DMSO was used as negative control. After 72 h incubation, 20 μ L of MTT (Meilune, China) solution was added to each well. After 4 h, the absorbance of each well was measured at wavelength of 490 nm on spectrophotometer. Data was corrected for background. IC₅₀ was calculated by GraphPad Prism 6.0 [52].

4.11. Analysis of apoptosis

Flow cytometric analysis based on the fluorochrome propidium iodide was performed as described previously. MGC803 was seeded at a density of 0.4 \times 10⁶ cells/well into 24-well plates and treated with induced concentration for 48 h, then cells were harvested and washed by PBS, and stained by Annexin V-FITC (Dojindo, Japan), PI (Dojindo, Japan) at room temperature. Then cells were analyzed by flow cytometry [53].

4.12. In vitro assay on HDAC1, HDAC6

OptiPlate-96 black microplates (PerkinElmer) were used for HDAC1 and HDAC6 enzyme activity assay in vitro. A series of compounds, SAHA were diluted with HDAC assay buffer containing 1% DMSO. Then human recombinant HDAC6 (BPS Bioscience, USA, catalog no. 50006) in incubation buffer, BSA, the fluorogenic substrate (Z-(Ac)-Lys-AMC) and the tested compounds were incubated in 96-well black plates at 37 °C for 40 min. After incubation, trypsin was added to release the fluorescent fragment of AMC for 15 min. The fluorescence intensity was measured with an excitation wavelength of 390 nm and emission wavelength of 460 nm. The IC₅₀ of the compounds was calculated and fitted by GraphPad prism 6.0 [54].

4.13. BioLayer interferometry (BLI)

HDAC6 (treated with NHS-LC-Biotin) at a concentration of 1 mg/mL was immobilized on SA sensors in kinetics buffer in 96-well black microplates (FortéBio, USA). The experiment was performed

on an Octet96 instrument (Pall, USA) at 25 °C. Activation was 50 s, immobilization of HDAC6 600 s, followed by washing for 300 s and then binding the compound **9r** for 300 s. Data was analyzed by the FortéBio Data Analysis 8.1 software (FortéBio, USA).

4.14. Cellular thermal shift assay (CETSA)

The interaction between HDAC6 and compound **9r** in vitro was further tested by the cellular thermal shift assay (CETSA). The technique can verify the binding of small molecules to corresponding target proteins for cellular level. Briefly, MGC803 was cultured in 6-well plate for 24 h and then were incubated with media containing DMSO or compound **9r** (4 μM) for 6 h. Cells were resuspended in ice-cold PBS and divided equally into 6 PCR tubes and lysed by repeated freezing and thawing heated. The lysate was heated at a temperature gradient from 44 °C to 54 °C for 3 min. Subsequently, the supernatant of the cells was analyzed by a Western blot assay.

4.15. Molecular docking study

The 3D structures of the compounds for docking were built using MOE 2015, and energy minimization was processed using the force field AMBER 10: EHT. The X-ray crystal structures of HDAC6 (PDB code 5EF7, 1.9 Å) was obtained from PDB database, and prepared with the QuickPrep module of MOE 2015 using the default parameters. The co-crystallized ligand of the protein was used to define the active site for docking. The default Triangle Matcher placement method was employed for docking, and GBVI/WSA dG scoring function was used to assess the free energy of binding of compound **9r** from a given pose and rank the final poses.

4.16. Western blot analysis

The MGC803 was treated with the induced concentration of compound **9r** for 48 h. Then cells were lysed with loading buffer (0.1% SDS 150 mM NaCl, 25 mM Tris-HCl, 1% deoxycholic acid sodium salt, 1% NP-40, 1% PMSF). After centrifuge, supernatant was collected and the protein concentration was quantized by the BCA Protein Quantitation Kit (Beyotime Biotechnology, China). Each sample was separated by 8–10% SDS/PAGE gels and transferred to a 0.22 μm PVDF membrane. After blocking in 5% non-fat dry milk at room temperature for 2 h, the membrane was incubated with the specific peroxidase-conjugated primary antibodies independently, Ac-α-tubulin (CST, USA), α-tubulin (CST, USA), Ac-H3 (Abcam, UK), H3 (Abcam, UK), Bcl-2 (Abcam, UK), Caspase 9 (Abcam, UK), Cleaved-Caspase 9 (Abcam, UK), PARP (Abcam, UK), Cleaved-PARP (Abcam, UK), GAPDH (Abcam, UK) overnight at 4 °C and followed by incubation with horseradish peroxidase conjugated secondary antibodies (Abcam, UK), and the ECL chemiluminescence detection kit (Meilune, China) was used and the chemiluminescence signal is then observed and collected in the dark using photosensitive film.

4.17. EdU cell proliferation assay

Cells treated by compound **9r** were placed in 24-well plate for 72 h. Then cells were treated with EdU cell proliferation kit (RiboBio, China) according to the manufacturer's instruction. Photograph was captured by fluorescence microscope to determine the effect of compound **9r** on cell proliferation.

4.18. Invasion assay

Cells were seeded in a Transwell 24-well plate with Matrigel (BD Bioscience, USA) with medium containing 1% FBS (upper chambers)

or medium containing 20% FBS (lower chambers). Meanwhile compound **9r** was added into the chamber. With 72 h incubation, the medium was abandoned, and the chambers were washed by PBS. Cell was fixed by 4% paraformaldehyde solution and stained with DAPI, and washed by PBS for three times. The chamber was photographed and analyzed by Molecular Devices (Thermo Fisher Scientific, USA).

4.19. Acute toxicity

8-10-week-old C57BL/6 mice (20 females and 20 males) were divided into two groups, respectively. One group served as negative control treated with corresponding solvent (0.5% CMC-Na). Another group was orally administrated compound **9r** on 2000 mg/kg a single time. For the observation of the following 14 days, the signs of toxicity (body weight, mortality, behavior) were recorded. Acute toxicity caused a set of experimental animals with 50% subject compounds dose was calculated for quantitative evaluation of death (LD50). And H&E staining of the lung, heart, liver, spleen and kidney tissue were assessed [54,55].

All animals were maintained in accordance with the Regulations of Experimental Animal Administration issued by the State Committee of Science and Technology of People's Republic of China.

4.20. Statistical analysis

All data are reported as means ± SD. Differences were analyzed by Student's t-test (with 95% confidence interval). p values < 0.05 were considered as statistically significant.

Declaration of competing interest

The authors declare that they have no known competing financial interests or personal relationships that could have appeared to influence the work reported in this paper.

Acknowledgement

This work was supported by National Natural Science Foundation of China (81703328 by Liying Ma; 81430085 and 81773562 by Hongmin Liu); National Key Research Program (2018YFE0195100 and 2016YFA0501800 by Hongmin Liu, China); Scientific Program of Henan Province (182102310070 by Liying Ma, China); China Postdoctoral Science Foundation (2020M672249 by Liying Ma); Henan Scientific Innovation Talent Team, Department of Education (19IRTSTHN001 by Zhao Wen, China).

Appendix A. Supplementary data

Supplementary data to this article can be found online at <https://doi.org/10.1016/j.ejmech.2021.113392>.

References

- [1] S. Zhao, W. Xu, W. Jiang, W. Yu, Y. Lin, T. Zhang, J. Yao, L. Zhou, Y. Zeng, H. Li, Y. Li, J. Shi, W. An, S.M. Hancock, F. He, L. Qin, J. Chin, P. Yang, X. Chen, Q. Lei, Y. Xiong, K.L. Guan, Regulation of cellular metabolism by protein lysine acetylation, *Science* 327 (2010) 1000–1004.
- [2] Y. Zhang, Z. Sun, J. Jia, T. Du, N. Zhang, Y. Tang, Y. Fang, D. Fang, Overview of histone modification, *Adv. Exp. Med. Biol.* 1283 (2021) 1–16.
- [3] G. Li, Y. Tian, W.G. Zhu, The roles of histone deacetylases and their inhibitors in cancer therapy, *Front. Cell Dev. Biol.* 8 (2020) 576946.
- [4] H. Yuan, R. Marmorstein, Structural basis for sirtuin activity and inhibition, *J. Biol. Chem.* 287 (2012) 42428–42435.
- [5] N.J. Porter, D.W. Christianson, Structure, mechanism, and inhibition of the zinc-dependent histone deacetylases, *Curr. Opin. Struct. Biol.* 59 (2019) 9–18.
- [6] F.A. Verza, U. Das, A.L. Fachin, J.R. Dimmock, M. Marins, Roles of histone deacetylases and inhibitors in anticancer therapy, *Cancers* 12 (2020) 1664.

- [7] T.C.S. Ho, A.H.Y. Chan, A. Ganesan, Thirty years of HDAC inhibitors: 2020 insight and hindsight, *J. Med. Chem.* 63 (2020) 12460–12484.
- [8] X. Lu, Z. Ning, Z. Li, H. Cao, X. Wang, Development of chidamide for peripheral T-cell lymphoma, the first orphan drug approved in China, *Intractable Rare Dis. Resear.* 5 (2016) 185–191.
- [9] Z.T. Rivers, D.R. Oostra, J.S. Westholder, G.M. Vercellotti, Romidepsin-associated cardiac toxicity and ECG changes: a case report and review of the literature, *J. Oncol. Pharm. Pract. : Off. Publ. Int. Soc. Oncol. Pharm. Pract.* 24 (2018) 56–62.
- [10] B.E. Gryder, Q.H. Sodji, A.K. Oyelere, Targeted cancer therapy: giving histone deacetylase inhibitors all they need to succeed, *Future Med. Chem.* 4 (2012) 505–524.
- [11] J.P. Laubach, F. Schjesvold, M. Mariz, M.A. Dimopoulos, E. Lech-Maranda, I. Spicka, V.T.M. Hungria, T. Shelekova, A. Abdo, L. Jacobasch, C. Polprasert, R. Hájek, Á. Illés, T. Wróbel, A. Sureda, M. Beksac, I.Z. Gonçalves, J. Bladé, S.V. Rajkumar, A. Chari, S. Lonial, A. Spencer, P. Maison-Blanche, P. Moreau, J.F. San-Miguel, P.G. Richardson, Efficacy and safety of oral panobinostat plus subcutaneous bortezomib and oral dexamethasone in patients with relapsed or relapsed and refractory multiple myeloma (PANORAMA 3): an open-label, randomised, phase 2 study, *The Lancet, Oncology* 22 (2021) 142–154.
- [12] J. Roche, P. Bertrand, Inside HDACs with more selective HDAC inhibitors, *Eur. J. Med. Chem.* 121 (2016) 451–483.
- [13] X.H. Zhang, M. Qin, H.P. Wu, M.Y. Khamis, Y.H. Li, L.Y. Ma, H.M. Liu, A review of progress in histone deacetylase 6 inhibitors Research: structural specificity and functional diversity, *J. Med. Chem.* 64 (2021) 1362–1391.
- [14] C.M. Grozinger, C.A. Hassig, S.L. Schreiber, Three proteins define a class of human histone deacetylases related to yeast Hda1p, *Proc. Natl. Acad. Sci. U.S.A.* 96 (1999) 4868–4873.
- [15] S. Pulya, S.A. Amin, N. Adhikari, S. Biswas, T. Jha, B. Ghosh, HDAC6 as privileged target in drug discovery: a perspective, *Pharmacol. Res.* 163 (2020) 105274.
- [16] Y.K. Kawaguchi, J.J. Kovacs, A. McLaurin, J.M. Vance, A. Ito, T.P. Yao, The deacetylase HDAC6 regulates aggresome formation and cell viability in response to misfolded protein stress, *Cell* 115 (2003) 727–738.
- [17] W.H. Choi, Y. Yun, S. Park, J.H. Jeon, J. Lee, J.H. Lee, S.A. Yang, N.K. Kim, C.H. Jung, Y.T. Kwon, D. Han, S.M. Lim, M.J. Lee, Aggresomal sequestration and STUB1-mediated ubiquitination during mammalian proteasome rephagy of inhibited proteasomes, *Proc. Natl. Acad. Sci. U. S. A.* 117 (2020) 19190–19200.
- [18] C. Hubbard, A. Guardia, R. Shao, Y. Kawaguchi, A. Ito, A. Nixon, M. Yoshida, X.F. Wang, T.P. Yao, HDAC6 is a microtubule-associated deacetylase, *Nature* 417 (2002) 455–458.
- [19] K. Ustinova, Z. Novakova, M. Saito, M. Meleshin, J. Mikesova, Z. Kutil, P. Baranova, B. Havlinova, M. Schutkowski, P. Matthias, C. Barinka, The disordered N-terminus of HDAC6 is a microtubule-binding domain critical for efficient tubulin deacetylation, *J. Biol. Chem.* 295 (2020) 2614–2628.
- [20] K. Messaoudi, A. Ali, R. Ishaq, A. Palazzo, D. Sliwa, O. Bluteau, S. Souquière, D. Muller, K.M. Diop, P. Rameau, V. Lapierre, J.P. Marolleau, P. Matthias, I. Godin, G. Pierron, S.G. Thomas, S.P. Watson, N. Droin, V. Vainchenker, I. Plo, H. Raslova, N. Debili, Critical role of the HDAC6-cortactin axis in human megakaryocyte maturation leading to a proplatelet-formation defect, *Nat. Commun.* 8 (2017) 1786.
- [21] J.Y. Kim, H.G. Hwang, J.Y. Lee, M. Kim, J.Y. Kim, Cortactin deacetylation by HDAC6 and SIRT2 regulates neuronal migration and dendrite morphogenesis during cerebral cortex development, *Mol. Brain* 13 (2020) 105.
- [22] J.J. Kovacs, P.J. Murphy, S. Gaillard, X. Zhao, J.T. Wu, C.V. Nicchitta, M. Yoshida, D.O. Toft, W.B. Pratt, T.P. Yao, HDAC6 regulates Hsp90 acetylation and chaperone-dependent activation of glucocorticoid receptor, *Mol. Cell* 18 (2005) 601–607.
- [23] R. Ojha, K. Nepali, C.H. Chen, K.H. Chuang, T.Y. Wu, T.E. Lin, K.C. Hsu, M.W. Chao, M.J. Lai, M.H. Lin, H.L. Huang, C.D. Chang, S.L. Pan, M.C. Chen, J.P. Liou, Isoindoline scaffold-based dual inhibitors of HDAC6 and HSP90 suppressing the growth of lung cancer in vitro and in vivo, *Eur. J. Med. Chem.* 190 (2020) 112086.
- [24] R.B. Parmigiani, W.S. Xu, G. Venta-Perez, H. Erdjument-Bromage, M. Yaneva, P. Tempst, P.A. Marks, HDAC6 is a specific deacetylase of peroxiredoxins and is involved in redox regulation, *Proc. Natl. Acad. Sci. U. S. A.* 105 (2008) 9633–9638.
- [25] T. Li, C. Zhang, S. Hassan, X. Liu, F. Song, K. Chen, W. Zhang, J. Yang, Histone deacetylase 6 in cancer, *J. Hematol. Oncol.* 11 (2018) 111.
- [26] F. Bray, J. Ferlay, I. Soerjomataram, R.L. Siegel, L.A. Torre, A. Jemal, Global cancer statistics 2018: GLOBOCAN estimates of incidence and mortality worldwide for 36 cancers in 185 countries, *Ca - Cancer J. Clin.* 68 (2018) 394–424.
- [27] I. Regel, L. Merkl, T. Friedrich, E. Burgermeister, W. Zimmermann, H. Einwächter, K. Herrmann, R. Langer, C. Rökken, R. Hofheinz, R. Schmid, M.P. Ebert, Pan-histone deacetylase inhibitor panobinostat sensitizes gastric cancer cells to anthracyclines via induction of CITED2, *Gastroenterology* 143 (2012) 99–109.
- [28] S.J. Park, J.K. Kim, H.J. Bae, J.W. Eun, Q. Shen, H.S. Kim, W.C. Shin, H.D. Yang, E.K. Lee, J.S. You, W.S. Park, J.Y. Lee, S.W. Nam, HDAC6 sustains growth stimulation by prolonging the activation of EGF receptor through the inhibition of rapabtin-5-mediated early endosome fusion in gastric cancer, *Canc. Lett.* 354 (2014) 97–106.
- [29] N. Wang, M. Chen, Z. Ni, T. Li, J. Zeng, G. Lu, J. Wang, J. Zhang, S. Wu, Y. Shi, HDAC6/HNF4 α loop mediated by miR-1 promotes bile acids-induced gastric intestinal metaplasia, *Gastr. Canc. Off. J. Int. Gastr. Canc. Assoc. Japanese Gastr. Canc. Assoc.* 24 (2021) 103–116.
- [30] R. Kaur, A.R. Dwivedi, B. Kumar, V. Kumar, Recent developments on 1,2,4-triazole nucleus in anticancer compounds: a review, *Anti Canc. Agents Med. Chem.* 16 (2016) 465–489.
- [31] A. Ayati, S. Emami, A. Foroumadi, The importance of triazole scaffold in the development of anticonvulsant agents, *Eur. J. Med. Chem.* 109 (2016) 380–392.
- [32] F. Gao, T. Wang, J. Xiao, G. Huang, Antibacterial activity study of 1,2,4-triazole derivatives, *Eur. J. Med. Chem.* 173 (2019) 274–281.
- [33] R. Aggarwal, G. Sumran, An insight on medicinal attributes of 1,2,4-triazoles, *Eur. J. Med. Chem.* 205 (2020) 112652.
- [34] A.A. Boezio, K. Andrews, C. Boezio, M. Chu-Moyer, K.W. Copeland, E.F. DiMauro, R.S. Foti, R.T. Freneau Jr., H. Gao, S. Geuns-Meyer, R.F. Graceffa, H. Gunaydin, H. Huang, D.S. La, J. Ligutti, B.D. Moyer, E.A. Peterson, Y. Yu, M.M. Weiss, 1,2,4-Triazolsulfone: a novel isosteric replacement of acylsulfonamides in the context of Na(V)1.7 inhibition, *Bioorg. Med. Chem. Lett* 28 (2018) 2103–2108.
- [35] D.Q. Xue, X.Y. Zhang, C.J. Wang, L.Y. Ma, N. Zhu, P. He, K.P. Shao, P.J. Chen, Y.F. Gu, X.S. Zhang, C.F. Wang, C.H. Ji, Q.R. Zhang, H.M. Liu, Synthesis and anticancer activities of novel 1,2,4-triazolo[3,4-a]phthalazine derivatives, *Eur. J. Med. Chem.* 85 (2014) 235–244.
- [36] S. Wang, Z.R. Li, F.Z. Suo, X.H. Yuan, B. Yu, H.M. Liu, Synthesis, structure-activity relationship studies and biological characterization of new [1,2,4] triazol[1,5-a]pyrimidine-based LSD1/KDM1A inhibitors, *Eur. J. Med. Chem.* 167 (2019) 388–401.
- [37] S. Wang, L. Zhao, X.J. Shi, L. Ding, L. Yang, Z.Z. Wang, D. Shen, K. Tang, X.J. Li, M. Mamun, H. Li, B. Yu, Y.C. Zheng, S. Wang, H.M. Liu, Development of highly potent, selective, and cellular active triazol[1,5-a]pyrimidine-based inhibitors targeting the DCN1-UBC12 protein-protein interaction, *J. Med. Chem.* 62 (2019) 2772–2797.
- [38] J.J. McClure, C. Zhang, E.S. Inks, Y.K. Peterson, J. Li, C.J. Chou, Development of allosteric hydrazide-containing class I histone deacetylase inhibitors for use in acute myeloid leukemia, *J. Med. Chem.* 59 (2016) 9942–9959.
- [39] X. Li, Y. Jiang, Y.K. Peterson, T. Xu, R.A. Himes, X. Luo, G. Yin, E.S. Inks, N. Dolloff, S. Halene, S.S.L. Chan, C.J. Chou, Design of hydrazide-bearing HDACs based on panobinostat and their p53 and FLT3-ITD dependency in antileukemia activity, *J. Med. Chem.* 63 (2020) 5501–5525.
- [40] Y. Li, F. Wang, X. Chen, J. Wang, Y. Zhao, Y. Li, B. He, Zinc-dependent deacetylase (HDAC) inhibitors with different zinc binding groups, *Curr. Top. Med. Chem.* 19 (2019) 223–241.
- [41] R. De Vreesse, M. D'Hooghe, Synthesis and applications of benzohydroxamic acid-based histone deacetylase inhibitors, *Eur. J. Med. Chem.* 135 (2017) 174–195.
- [42] W. Doherty, E.M. Dürr, H.T. Baddock, S.Y. Lee, P.J. McHugh, T. Brown, M.O. Senger, E.M. Scanlan, J.F. McGouran, A hydroxamic-acid-containing nucleoside inhibits DNA repair nuclease SNM1A, *Org. Biomol. Chem.* 17 (2019) 8094–8105.
- [43] J.D. Osko, D.W. Christianson, Structural determinants of affinity and selectivity in the binding of inhibitors to histone deacetylase 6, *Bioorg. Med. Chem. Lett* 30 (2020) 127023.
- [44] J.K. Kyle, V. Butler, Camille Brochier, Giulio Vistoli, Brett Langley, Alan P. Kozikowski, Rational design and simple chemistry yield a superior, neuroprotective HDAC6 inhibitor, Tubastatin A, *J. Am. Chem. Soc.* 132 (2010) 10842–10846.
- [45] J. Dong, N. Zheng, X. Wang, C. Tang, P. Yan, H.B. Zhou, J. Huang, A novel HDAC6 inhibitor exerts an anti-cancer effect by triggering cell cycle arrest and apoptosis in gastric cancer, *Eur. J. Pharmacol.* 828 (2018) 67–79.
- [46] Y.W. Song, Y. Lim, S.K. Cho, 2,4-Di-tert-butylphenol, a potential HDAC6 inhibitor, induces senescence and mitotic catastrophe in human gastric adenocarcinoma AGS cells, *Biochimica et biophysica acta, Mol. Cell Resear.* 1865 (2018) 675–683.
- [47] J. Sun, J. Piao, N. Li, Y. Yang, K.Y. Kim, Z. Lin, Valproic acid targets HDAC1/2 and HDAC1/PDEN/Akt signalling to inhibit cell proliferation via the induction of autophagy in gastric cancer, *FEBS J.* 287 (2020) 2118–2133.
- [48] Q. Shen, W. Tang, J. Sun, L. Feng, H. Jin, X. Wang, Regulation of CRADD-caspase 2 cascade by histone deacetylase 1 in gastric cancer, *Am. J. Tourism Res.* 6 (2014) 538–547.
- [49] A. Singh, T.Y. Chang, N. Kaur, K.C. Hsu, Y. Yen, T.E. Lin, M.J. Lai, S.B. Lee, J.P. Liou, CAP rigidification of MS-275 and chidamide leads to enhanced anti-proliferative effects mediated through HDAC1, 2 and tubulin polymerization inhibition, *Eur. J. Med. Chem.* 215 (2021) 113169.
- [50] Y. Hai, D.W. Christianson, Histone deacetylase 6 structure and molecular basis of catalysis and inhibition, *Nat. Chem. Biol.* 12 (2016) 741–747.
- [51] J.D. Osko, D.W. Christianson, Structural determinants of affinity and selectivity in the binding of inhibitors to histone deacetylase 6, *Bioorg. Med. Chem. Lett* 30 (2020) 127023.
- [52] Z.X. He, J.L. Huo, Y.P. Gong, Q. An, X. Zhang, H. Qiao, F.F. Yang, X.H. Zhang, L.M. Jiao, H.M. Liu, L.Y. Ma, W. Zhao, Design, synthesis and biological evaluation of novel thiosemicarbazone-indole derivatives targeting prostate cancer cells, *Eur. J. Med. Chem.* 210 (2021) 112970.
- [53] K. Vögler, N. Ong, J. Senger, D. Herp, K. Schmidt-kunz, M. Marek, M. Müller, K. Bartel, T.B. Shaik, N.J. Porter, D. Robaa, D.W. Christianson, C. Romier, W. Sippl, M. Jung, F. Bracher, Synthesis and biological investigation of phenothiazine-based benzhydroxamic acids as selective histone deacetylase 6

- inhibitors, *J. Med. Chem.* 62 (2019) 1138–1166.
- [54] J.H. Lee, A. Mahendran, Y. Yao, L. Ngo, G. Venta-Perez, M.L. Choy, N. Kim, W.S. Ham, R. Breslow, P.A. Marks, Development of a histone deacetylase 6 inhibitor and its biological effects, *Proc. Natl. Acad. Sci. U. S. A.* 110 (2013) 15704–15709.
- [55] Y. Gao, L. Zhu, J. Guo, T. Yuan, L. Wang, H. Li, L. Chen, Farnesyl phenolic enantiomers as natural MTH1 inhibitors from *Ganoderma sinense*, *Oncotarget* 8 (2017) 95865–95879.